AMSR Land Surface Parameters

Surface Soil Moisture • Land Surface Temperature • Vegetation Water Content

ALGORITHM THEORETICAL BASIS DOCUMENT

Version 3.0

Eni G. Njoku

Jet Propulsion Laboratory, M/S 300-233
4800 Oak Grove Drive, Pasadena, CA 91109
Phone: (818) 453-3693
Fax: (818) 354-9476
E-mail: eni.g.njoku@jpl.nasa.gov

December 10, 1999

Jet Propulsion Laboratory
California Institute of Technology
Pasadena, CA

CONTENTS

CONTENTS 2

1. INTRODUCTION 3

2. OVERVIEW AND BACKGROUND 4

2.1 EXPERIMENT OBJECTIVES 6
2.2 HISTORICAL PERSPECTIVE 6
Soil Moisture and Flooding *7*
Surface Temperature *8*
Surface Vegetation *8*
Heterogeneous Surfaces *8*
Integration of Retrievals with Soil-Vegetation Modeling *11*
2.3 INSTRUMENT CHARACTERISTICS 11
2.3.1 Instrument Description 11
2.3.2 Instrument Calibration 11
2.3.3 Data Products 12

3. ALGORITHM DESCRIPTION 13

3.1 THEORETICAL DESCRIPTION 13
3.1.1 Physics of the Problem 13
Atmosphere *15*
Surface *15*
Model Summary *17*
Effects of Inhomogeneity *18*
Model Calibration *24*
Sensitivities *25*
3.1.2 Mathematical Description of the Algorithm 25
Baseline Algorithm *26*
Enhanced Algorithms *29*
3.1.3 Variance and Uncertainty Estimates 29
Simulation Studies *29*
Tests Using SMMR Data *30*
3.2 PRACTICAL CONSIDERATIONS 34
3.2.1 Numerical Computation Considerations 34
3.2.2 Programming/Procedural Considerations 34
3.2.3 Calibration and Validation 35
Model Calibration *35*
Validation Issues *35*
Validation Sites and Methodology *39*
Global Scale Validation *43*
3.2.4 Quality Control and Diagnostics 43
3.2.5 Exception Handling 43

4. CONSTRAINTS, LIMITATIONS, AND ASSUMPTIONS 44

5. REFERENCES 44

1. INTRODUCTION

The Advanced Microwave Scanning Radiometer on EOS (AMSR-E) is a multichannel passive microwave instrument scheduled to be launched on the Earth Observing System (EOS) Aqua satellite in December 2000. The AMSR-E instrument was developed by the National Space Development Agency (NASDA) of Japan, and is a modified form of the AMSR instrument that will be launched on the Japanese Advanced Earth Observing Satellite-II (ADEOS-II) in 2001.

The two AMSR instruments will operate in polar, sun-synchronous orbits, with equator crossings at 10:30 am and 1:30 pm for ADEOS-II and Aqua respectively. The AMSR is a successor in technology to the Scanning Multichannel Microwave Radiometer (SMMR) and Special Sensor Microwave Imager (SSM/I) instruments, first launched in 1978 and 1987 respectively, and will provide observations of variables describing the Earth's atmosphere, ocean, cryosphere, and land surface. Over snow-free land, it will be possible to estimate three surface variables from AMSR data—surface soil moisture m_e, vegetation water content w_e, and land-surface temperature T_e. Soil moisture is of primary importance in MTPE studies and is a standard product of this investigation. Surface temperature and vegetation water content are also important MTPE requirements and are included as research products.

This document describes the algorithm and validation approach for the AMSR land products. The products are applicable to surface energy and water balance studies, large-scale hydrologic modeling, numerical weather prediction, climate modeling, and monitoring of floods, droughts, and land-cover change. These studies are part of the MTPE "Seasonal-to-Interannual Climate Variability and Prediction" and "Natural Hazards" research objectives, and will contribute to the "Land-Cover and Land-Use Change" and "Long-Term Climate" research objectives (MTPE, 1996).

The algorithm for deriving m_e, T_e, and w_e from AMSR data is based on a physical model of microwave emission from a layered soil-vegetation-atmosphere medium. The model is derived from theory and experimental data, and is considered to be valid at frequencies up to ~10 GHz. Soil emission is masked to a significant degree by vegetation at frequencies above ~10 GHz, thus the retrieval algorithm uses the two lowest frequencies of AMSR (6.9 and 10.7 GHz). The higher frequencies (18 and 37 GHz) are used for surface classification as a preliminary step in the geophysical retrievals. An iterative, least-squares-minimization method is employed in the retrieval algorithm. The retrieved variables represent area-averages over the 6.9-GHz footprints. The retrievals of m_e and T_e also represent averages over the respective vertical sampling depths in the soil/vegetation medium. As the vegetation cover increases, the retrieval errors for m_e and w_e increase. For dense vegetation these variables cannot be retrieved. The retrieval algorithm identifies when the reliability threshhold has been exceeded. Evaluation of the derived products will be performed in conjunction with associated EOS interdisciplinary investigations and international programs such as GEWEX.

2. OVERVIEW AND BACKGROUND

Routine global measurement of soil moisture, leading to better understanding of large-scale land-surface hydrologic processes, is a high priority for EOS. Earth system modeling will benefit from remotely sensed soil moisture information for assimilations and comparisons with weather and climate and land surface hydrologic models, and for monitoring floods and droughts.

Measurements of land-surface temperature and vegetation cover are needed for surface-flux process studies and climate and ecosystem modeling. AMSR measurements of these variables will complement similar measurements using optical and thermal infrared sensors on EOS (MODIS and AIRS). Although passive-microwave measurements have lower spatial resolution they are less affected by aerosols and clouds, and are responsive to different dynamic ranges of vegetation structure and biomass than optical and infrared measurements. There is potential for improved synergistic products of surface temperature and vegetation using combined microwave, infrared, and optical data.

Soil moisture (surface wetness), vegetation dynamics, and surface temperature are three of the twenty-four measurements identified as high priorities by the MTPE program (MTPE, 1996). The AMSR land products generated by this investigation will address directly and uniquely these three critical areas.

Several studies during the past few years have investigated the influence of soil moisture on the atmospheric boundary layer (e.g. Brubaker and Entekhabi, 1996) and have provided insights into the importance of soil moisture in controling the feedbacks between land surface and atmosphere that influence climate (Shukla and Mintz, 1982; Delworth and Manabe, 1989). Improved characterizations of soil moisture, surface temperature, and vegetation cover in numerical weather prediction models have been shown to provide significant improvement in forecast skills. Figure 1 shows the large impact of wet versus dry initial soil moisture conditions on 30-day precipitation forecasts using the European Centre for Medium-range Weather Forecasts (ECMWF) model (Beljaars et al., 1996). The lack of a global observational capability to provide information on the temporal and spatial variability of the soil moisture, surface temperature, and vegetation cover is a major impediment to progress in forecasting. The AMSR land products can thus make an important contribution to the suite of MTPE/EOS measurements.

The terminologies and parameterizations used in describing land surface states are not well defined or consistently applied. The term ‘soil wetness’ is commonly used to describe the amount of soil water computed from a land-surface model, i.e. a soil-vegetation-atmosphere (or ‘SVAT’) moisture- and heat-flux model with given atmospheric forcing. However, soil wetness so defined is often model dependent—different SVAT models can give different values of soil wetness while having similar estimates of water and energy exchange. Also the soil depth within which the soil wetness is defined varies according to the model (Wei, 1995). For surface temperature, the terms ‘canopy temperature’, ‘skin temperature’, ‘aerodynamic temperature’, and ‘radiation temperature’

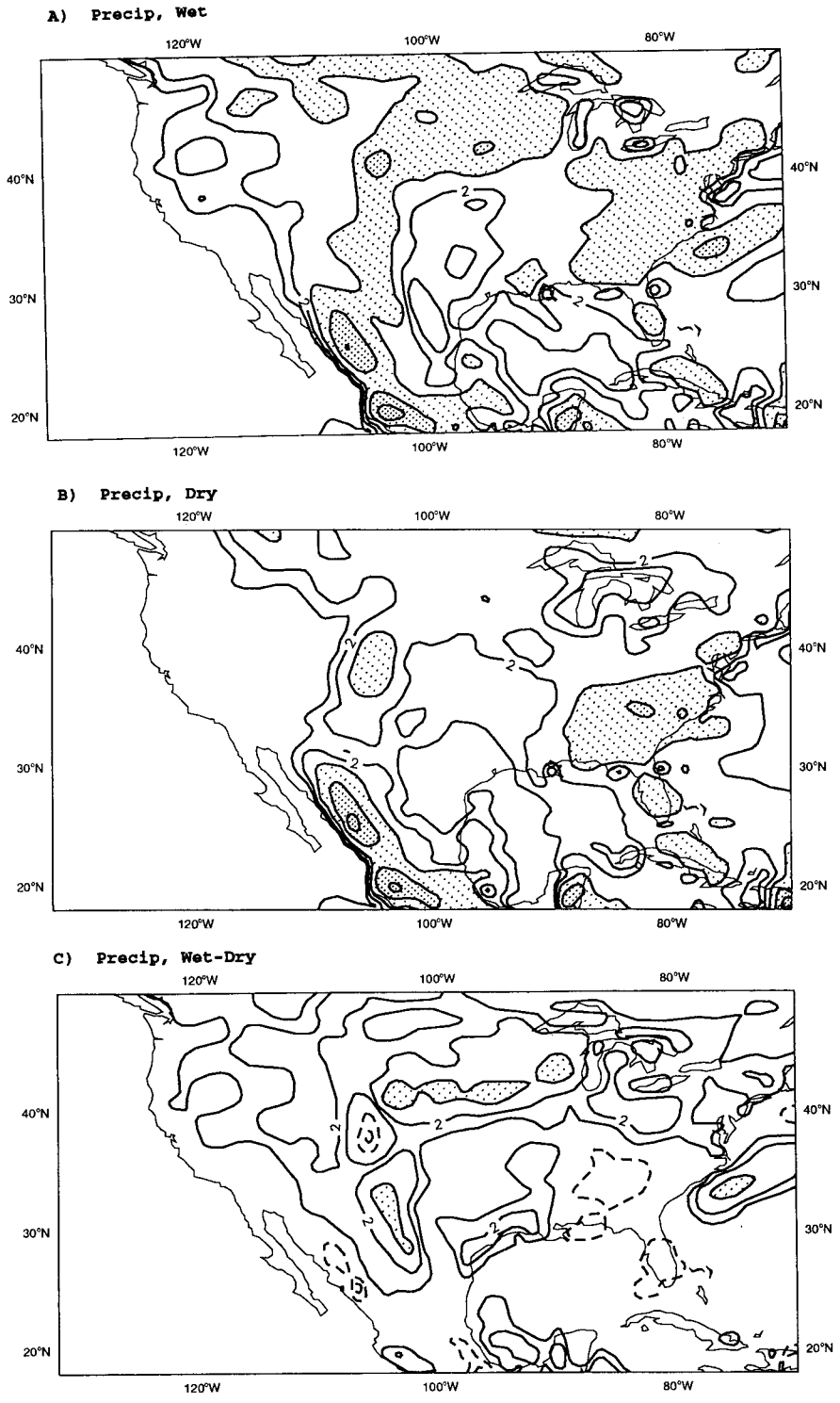

Figure 1: Precipitation averaged over an ensemble of three 30-day forecasts for July 1993 using the ECMWF model. (a) Moist initial soil moisture (field capacity). (b) Dry initial soil moisture (25% availability). (c) Difference between moist and dry. Contours are at 1, 2, 4, and 8 mm day^{-1} with shading above 4 mm day^{-1}. (From Beljaars et al., 1996.)

may be implied depending on the context, e.g. the SVAT model being used, the viewing direction and wavelength of the sensor, or the 3-dimensional characteristics of the surface (Norman and Becker, 1995). Likewise, various parameters have been used to describe vegetation cover, including 'biomass', 'leaf-area index (LAI)', 'normalized difference vegetation index (NDVI)', etc. In this document we attempt to provide clear definitions of the AMSR-derived variables m_e, T_e, and w_e. Coupled remote sensing and land surface modeling may ultimately provide the best means for utilizing the remote sensing measurements.

2.1 EXPERIMENT OBJECTIVES

The principal objective is to provide global remotely-sensed land surface measurements for use by the MTPE research and operational forecasting communities. The key land-surface variables that can be derived from AMSR are surface soil moisture m_e, land-surface temperature T_e, and vegetation water content w_e. Soil moisture is the primary measurement objective of this investigation. Surface temperature and vegetation water content are estimated by the algorithm as part of the soil moisture retrieval. All three variables are high-priority measurements in their own rights for climate and ecological modeling and monitoring purposes. The main objectives can be summarized as follows:

- Derive a self-consistent set of land surface variables m_e, T_e, and w_e, with global coverage (except for regions of open water, dense vegetation, frozen ground, snow cover, and mountainous terrain) from AMSR data. The variables will be estimated at a spatial resolution of approximately 70 km (the spatial resolution of the lowest AMSR frequency). Provide accuracy estimates for the retrieved variables.

- Validate the accuracies of the derived products, and document the algorithms, caveats, and data descriptions necessary for researchers to utilize the data quantitatively in scientific studies.

- Make the data products, algorithms, and metadata available through EOSDIS.

- Promote use of the derived products for: (a) improved understanding of macroscale land-surface hydrologic processes; (b) validating and initializing climate and weather prediction models; and (c) monitoring land surface change and climatic anomalies (including floods and droughts).

2.2 HISTORICAL PERSPECTIVE

To date, rather limited attention has been paid to the use of spaceborne passive microwave data for land sensing. Previous microwave radiometers have been sub-optimal in terms of spatial resolution and frequency range, particularly for soil moisture sensing. The Scanning Multichannel Microwave Radiometer (SMMR) launched on the Nimbus-7 satellite in 1978 had a spatial resolution of ~140 km at its lowest frequency of 6.6 GHz. The Special Sensor Microwave Imager (SSM/I) launched in 1987 has a lowest frequency of 19.3 GHz, at which moderate amounts of vegetation largely mask the soil moisture signal. The SMMR and SSM/I were designed for ocean, atmosphere, and cryosphere studies. Low frequencies (~1 to 3 GHz) are preferable for soil moisture sensing since attenuation through vegetation is less at longer wavelengths and the

Table 1: Comparative operating characteristics of SMMR, SSM/I, and AMSR

Parameter	SMMR (Nimbus-7)	SSM/I (DMSP)	AMSR (EOS)
Frequencies (GHz)	6.6, 10.7, 18, 21, 37	19.3, 22.3, 37, 85.5	6.9, 10.7, 18.7, 23.8, 36.5, 89
Altitude (km)	955	860	705
Antenna size (m)	0.79	0.6	1.6
Incidence angle (deg)	50.3	53.1	55
Footprint size (km)			
at ~7 GHz	140	N/A	70
at ~37 GHz	27	35	14
Swath width (km)	780	1400	1445
Launch date	(1978—No longer operating)	(1987—Series in orbit)	2000

sensitivity to moisture in the top few centimeters of soil is greater. The 6.6 and 10.7 GHz channels of the SMMR (similar to the low-frequency AMSR channels) have been shown, however, to be sensitive to surface soil moisture under low-vegetation conditions. The improved spatial resolution provided by AMSR (~70 km) is reasonably matched to the grid scales of the global atmospheric general circulation models (~50-100 km). Thus, AMSR will provide the first opportunity to obtain quantitative soil moisture data for global hydrologic and climate studies. The comparative performance characteristics of the SMMR, SSM/I, and AMSR are shown in Table 1.

The potential of the 6.6 and 10.7 GHz channels of the SMMR for soil moisture estimation was first investigated by Wang (1985) and Njoku and Patel (1986). These studies were followed by others (Owe et al., 1988; Choudhury and Golus, 1988; Kerr and Njoku, 1990; Owe et al., 1992; and van de Griend and Owe, 1994). The SMMR was also shown to be useful for monitoring seasonal flooding (Sippel et al., 1994), and for vegetation monitoring (Choudhury et al., 1987; Calvet et al., 1994). McFarland et al. (1990), Calvet et al. (1994), and Njoku(1995a) showed that SMMR and SSM/I data could be used to estimate surface temperature. The effects of the intervening atmosphere on land-surface measurements at 37 GHz were investigated by Choudhury et al. (1992) and Kerr and Njoku (1993). Ferraro et al. (1986), Neale et al. (1990) and others have investigated surface type classifications obtainable using SMMR and SSM/I data. These investigations, and others, have indicated the potential of AMSR for land surface studies.

Soil Moisture and Flooding

Estimates of large-scale surface soil moisture for comparison with satellite observations can be derived from precipitation and surface meteorological data coupled with models of surface energy and water balance. Such estimates are currently produced by numerical forecast models (e.g. NCEP and ECMWF) using four-dimensional data assimilation (4DDA). An earlier method was the Antecedent Precipitation Index (API) which has been commonly used as a soil wetness index.

Shown in Figure 2(a) are SMMR brightness temperatures T_B at 6.6 GHz horizontal polarization over two regions in Kansas and Texas plotted as a function of API for five years of data between the months of May and August (Choudhury and Golus, 1988). The relationship between API and T_B is evident. The Texas region (Quadrant (1,3)) has less vegetation and hence the data show a steeper slope (greater sensitivity to surface moisture).

Owe and van de Griend (1990) used a land-surface model to estimate large-area soil moisture from precipitation measurements in Botswana (Figure 2(b)). Figure 2(c) shows their comparisons of SMMR-derived surface emissivity at 6.6 GHz versus soil moisture in the top 10 cm, using corrections for vegetation obtained from AVHRR Normalized Difference Vegetation Index (NDVI) data (van de Griend and Owe, 1994). The model-based surface soil moisture estimates rely on sparsely-sampled precipitation data and may not represent well the moisture conditions in the top centimeter of soil at the time of the satellite overpass. Nevertheless, good correlations are obtained between the spaceborne microwave observations and the surface soil moisture.

Surface Temperature

Microwave surface temperature retrievals were tested over the U.S. using linear regression algorithms developed for SSM/I (McFarland et al., 1990). Comparison data used were surface air-temperatures obtained in the early morning hours close to the times of the satellite overpasses. Accuracies of 2 to 2.5°C were obtained (Figure 3(a)) which were supported by results of simulation studies (Njoku, 1995a) (Figure 3(b)). Other studies over forested regions have been reported by Calvet et al. (1994) and Pulliainen et al. (1997).

Surface Vegetation

Vegetation studies using spaceborne microwave radiometry have focused mainly on the use of a qualitative index consisting of the difference ΔT between vertically and horizontally polarized brightness temperatures at 37 GHz (Choudhury et al., 1987; Townshend et al., 1989). This index is simple to compute, and the higher spatial resolution at 37 GHz is advantageous. Unfortunately, the index is not directly related to a physical vegetation quantity. Vegetation opacity on the other hand is a parameter of the radiative transfer equation, and at 6–10 GHz is approximately linearly related to the vegetation water content. Thus, it is possible to make quantitative estimates in this frequency range of the vegetation water content (which is related to the vegetation biomass). It is also advantageous to use the lower frequencies in order to cover a larger dynamic range of biomass without saturation.

Heterogeneous Surfaces

The effects of mixed surface types within the sensor footprints must be taken into account due to the heterogeneity of land surfaces. Retrievals of surface parameters will represent nonlinear averages of the component quantities making up the scene—except where vegetation is low, in which case the averages will be approximately linear (Njoku et al., 1995b). The effect of nonlinearity is only significant, however, where vegetation and bare soil regions of large emissivity contrast cover the footprint in comparable fractions. The issue of how averaging affects the usefulness of the estimates for hydrologic modeling is important, and depends on the

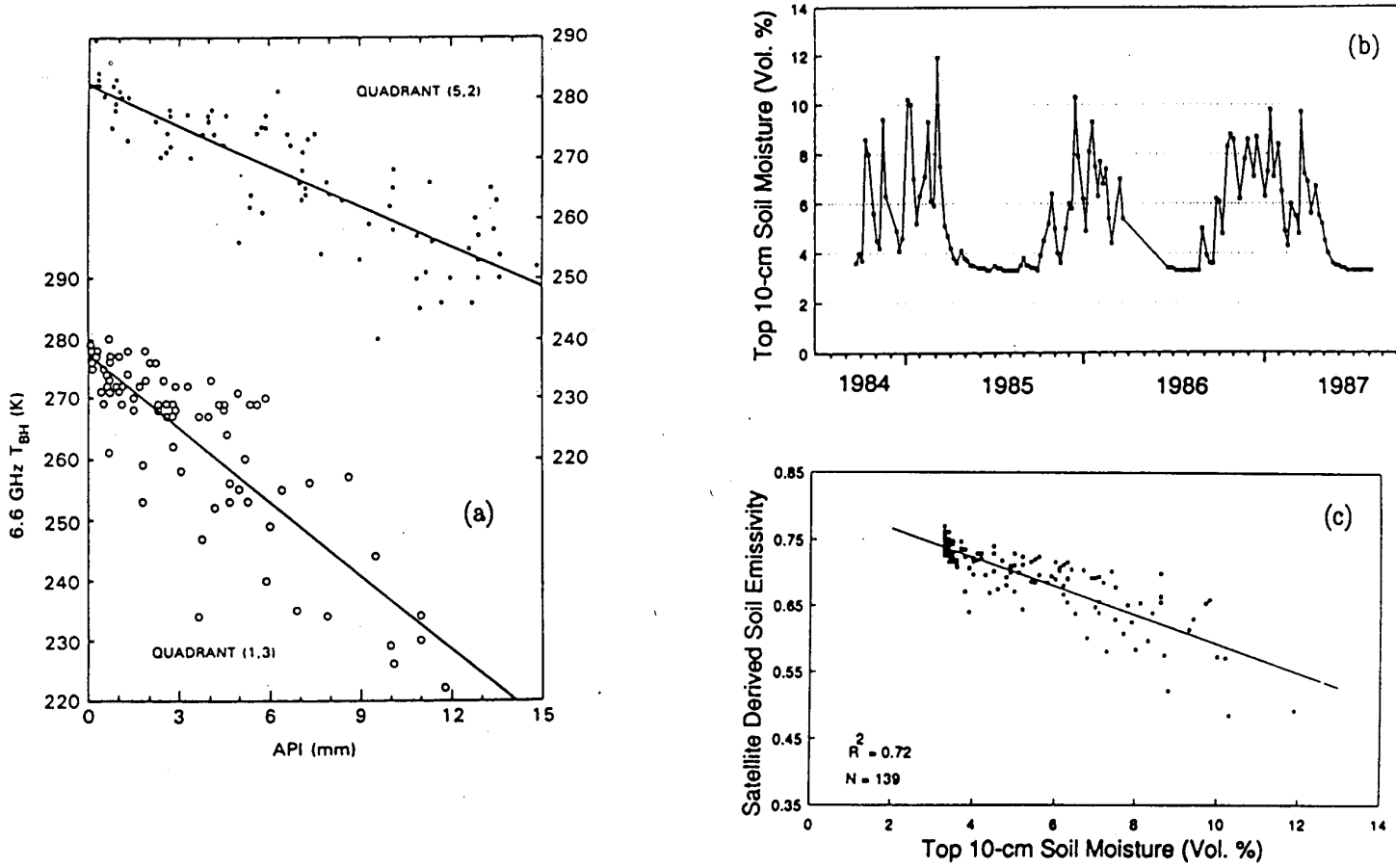

Figure 2: (a) Brightness temperature response to surface moisture (antecedent precipitation index) at 6.6 GHz using SMMR spaceborne observations, for surfaces of different vegetation cover (Choudhury and Golus, 1988). (b) Large-area soil moisture derived from in situ data and soil model for times of SMMR overpasses; and (c) relationship between SMMR-derived surface emissivity and soil moisture after correction for vegetation (van de Griend and Owe, 1994).

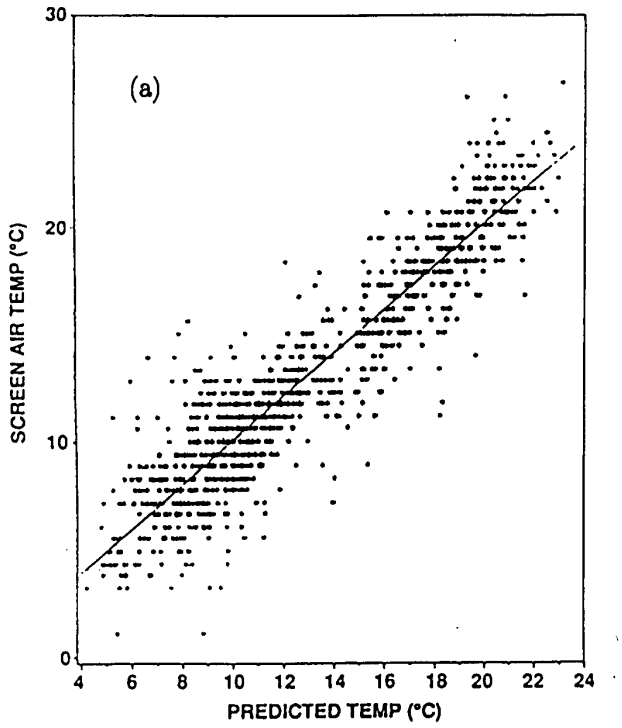

Regression Coefficients and Statistics for 4-Channel Model:

Land Surface Type	R^2	RMSE	Intercept	85 V	37 V	22 V	19 H
Crops/range	0.81	2.58	22.40	1.239	-0.396	0.275	-0.174
Moist soils	0.85	1.99	41.69	1.245	-0.724	0.415	-0.063
Dry soils	0.62	2.60	76.28	-0.367	-0.318	1.408	0.025
All	0.79	2.37	58.07	0.811	-0.555	0.730	-0.170

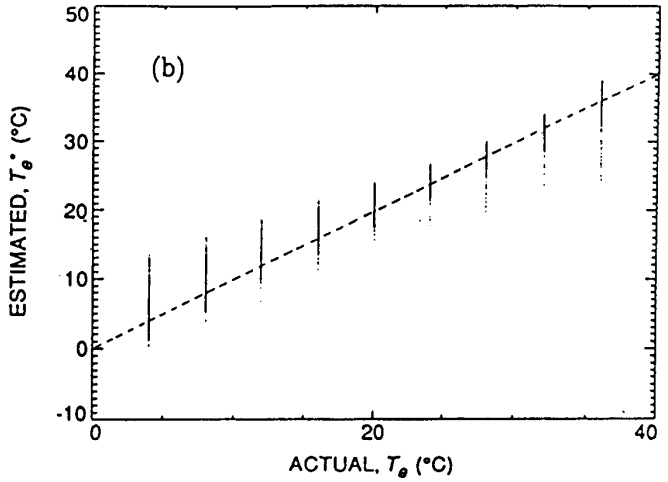

Figure 3: (a) Surface air temperature versus retrieved land surface temperature using SSM/I observations (McFarland et al., 1990). (b) Simulated linear regression retrievals of land surface temperature, using SMMR, for surfaces including vegetation ranging from 0 to 2 kg m^{-2} water content.

parameterization schemes of the hydrologic models. Much attention has been paid recently to this aspect (e.g. Lhomme et al., 1994; Raupach and Finnigan, 1995).

Integration of Retrievals with Soil-Vegetation Modeling

A number of studies have considered approaches in which microwave radiances are assimilated directly into predictive models of moisture and heat flow in soils and ecosystem functioning (Entekhabi et al., 1994; LoSeen et al, 1995; Liou and England, 1996). Microwave radiative transfer models coupled with models of heat and moisture fluxes in soils can be used to retrieve higher-level products such as subsurface moisture and temperature profile information and surface heat fluxes. Such products are exploratory and will be developed as research products.

2.3 INSTRUMENT CHARACTERISTICS

2.3.1 Instrument Description

The AMSR is a passive microwave instrument that measures brightness temperature at six frequencies, 6.925, 10.65, 18.7, 23.8, 36.5, and 89.0 GHz, with vertical and horizontal polarizations at each frequency for a total of twelve channels. The EOS AMSR is a modified version of the AMSR developed for ADEOS-II, and consists of a 1.6-m-diameter offset parabolic reflector fed by an array of six feedhorns. The reflector and feedhorn array are mounted on a drum which also contains the radiometers and mechanical and electronic subsystems. The reflector/feed/drum assembly rotates around the vertical axis using a coaxially-mounted bearing and power-transfer assembly. All data, commands, timing and telemetry signals, and power pass through the assembly on slip-ring connectors.

A cold-sky reflector and a warm load are mounted on the transfer-assembly shaft and do not rotate with the drum assembly. They are positioned off-axis such that they pass between the feedhorn array and the parabolic reflector once each scan. The cold-sky reflector reflects sky radiation into the feedhorn array. This, and the warm load, serve as calibration references. Corrections for antenna pattern spillover and cross-polarization effects are incorporated in the level 1 processing algorithms.

The AMSR rotates continuously at 40 rpm (i.e. with a period of 1.5 s). At an altitude of 705 km it measures the upwelling scene brightness temperatures over an angular sector of ± 61° about the sub-satellite track, resulting in a swath width of 1445 km. During the period of 1.5 seconds the spacecraft sub-satellite point travels 10 km. Even though the instantaneous fields-of-view are different for each channel, scene measurements are recorded at equal intervals of 10 km (5 km for the 89 GHz channels) along the scan. The half-cone offset angle of the reflector is 47.4° which results in an Earth-incidence angle of 55°. Table 2 lists the pertinent performance characteristics.

2.3.2 Instrument Calibration

The accuracy of the AMSR brightness temperature measurements includes the rms accuracy or sensitivity ΔT and the absolute calibration accuracy. The sensitivity per sample for each frequency is shown in Table 2, and is a function of the receiver noise temperature, integration time, and

Table 2. EOS AMSR Nominal Performance Characteristics

Center Frequencies (GHz)	6.925	10.65	18.7	23.8	36.5	89.0
Bandwidth (MHz)	350	100	200	400	1000	3000
Sensitivity (K)	0.3	0.6	0.6	0.6	0.6	1.1
IFOV (km)	76 x 44	49 x 28	28 x 16	31 x 18	14 x 8	6 x 4
Sampling Rate (km)	10 x 10	10 x 10	10 x 10	10 x 10	10 x 10	5 x 5
Integration Time (ms)	2.6	2.6	2.6	2.6	2.6	1.3
Main Beam Efficiency (%)	95.3	95.0	96.3	96.4	95.3	96.0
Beamwidth (degrees)	2.2	1.4	0.8	0.9	0.4	0.18

bandwidth. The radiometer calibration accuracy budget, exclusive of antenna pattern correction effects, is comprised of three major contributions: a warm load reference error, a cold load reference error, and radiometer nonlinearities and errors. Accounting for all errors, the total estimated sensor bias error, as provided by the instrument manufacturer, is 0.66 K at 100 K, increasing slightly with temperature to 0.68 K at 250 K.

The major part of the warm-load reference error comes from the following four components: (a) the accuracy of the platinum resistance thermistors (PRTs) as measured by the manufacturer—on of the order of ± 0.1 K; (b) the temperature gradient over the load area (the SSM/I gradient reached values as high as ±0.4 K); (c) load–feedhorn coupling errors due to the design of the system; and (d) reflections out of the feedhorn due to receiver electronics. An estimate of the warm load reference error, taking the root-sum-squared of the aforementioned components, is ±0.5 K. The error in the cold reference measurement is caused mainly by the residual error in coupling between the cold sky reflector and the feedhorn. This is estimated to be ±0.5 K. Other factors affecting the cold reference error are the reflections out of the feedhorn due to the receiver electronics, and the resistive losses of the cold sky reflector itself. An estimate of this error can be as high as ±0.62 K.

The main factor influencing radiometer nonlinearity is imperfect operation of the square law detector. This nonlinearity results in an error that can be estimated during the thermal-vacuum calibration testing. (On SSM/I this error was ±0.4 K.) Another source of error in the receiver electronics is the gain drift caused by instrument temperature variation over one orbit. This error depends on the design of the receiver and the overall design of the sensor. The drift can be as high as ±0.24 K for a temperature variation of less than 10 °C over one orbit.

2.3.3 Data Products

The data products of this investigation are summarized in Table 3. These output products will be generated from the input level 2a data. AMSR level 2a data (see the AMSR Level 2a ATBD) are calibrated, co-registered, comensurate brightness temperatures, such that for given subsets of channels, the brightness temperatures of all channels represent the same spatial regions on the ground (the effective antenna patterns and sampling locations are the same). The level 2a product is used as our starting point since the retrieval algorithm assumes that at each retrieval point the

multichannel brightness temperatures are characteristic of the same region of terrain (i.e. they have the same footprint size and location). The gridded brightness temperatures will be archived for use in further research algorithm development.

Table 3: AMSR Land-Surface Products

Product Type, Level[Ψ]	Parameter	Estimated Accuracy	Spatial Resolution[ξ]	Grid Resolution[†]	Granularity
S, 2	Surface soil moisture	0.06 g cm^{-3} [ζ]	60 km	25 km	half-orbit
R, 2	Vegetation water content	0.15 kg m^{-2} [ζ]	60 km	25 km	half-orbit
R, 2	Surface temperature	2.5 C	60 km	25 km	half-orbit
S, 3	Brightness temperatures	0.3–0.6 K	11, 60 km	25 km	1 day[η]
S, 3	Surface soil moisture	0.06 g cm^{-3} [ζ]	60 km	25 km	1 day[η]
R, 3	Vegetation water content	0.15 kg m^{-2} [ζ]	60 km	25 km	1 day[η]
R, 3	Surface temperature	2.5 C	60 km	25 km	1 day[η]

[Ψ] S = standard; R = research; 2 = level 2; 3 = level 3
[ξ] Mean footprint size, see Table 2
[†] Nominal grid spacing
[ζ] For vegetation water content <1.5 kg m^{-2}
[η] Ascending and descending separate

3. ALGORITHM DESCRIPTION

3.1 THEORETICAL DESCRIPTION

The retrieval algorithm for m_e, T_e, and w_e uses a physically-based radiative transfer model. The level of detail in the model is appropriate to the spatial scale of the AMSR footprints and the uncertainty in knowledge of the physical processes involved. Errors in physical modeling and uncertainties in model parameters will propagate as retrieval errors in the inversions. Modeling surface roughness and vegetation scattering effects requires increasing complexity above ~10 GHz, and the uncertainty is greater. Hence, our baseline algorithm uses the two lowest AMSR frequencies (6.9 and 10.7 GHz). These frequencies also have better vegetation penetration and soil moisture sensitivity though at the cost of decreased spatial resolution. The 18 and 37 GHz channels are used for surface classification as a preliminary step in the retrievals.

3.1.1 Physics of the Problem

The land surface is modeled as an absorbing vegetation layer above soil (Figure 4). The brightness temperature T_{B_p} observed at the top of the atmosphere at a given incidence angle and at a given frequency can be expressed by the radiative transfer equation (e.g. Mo et al., 1982; Kerr and Njoku, 1990) as:

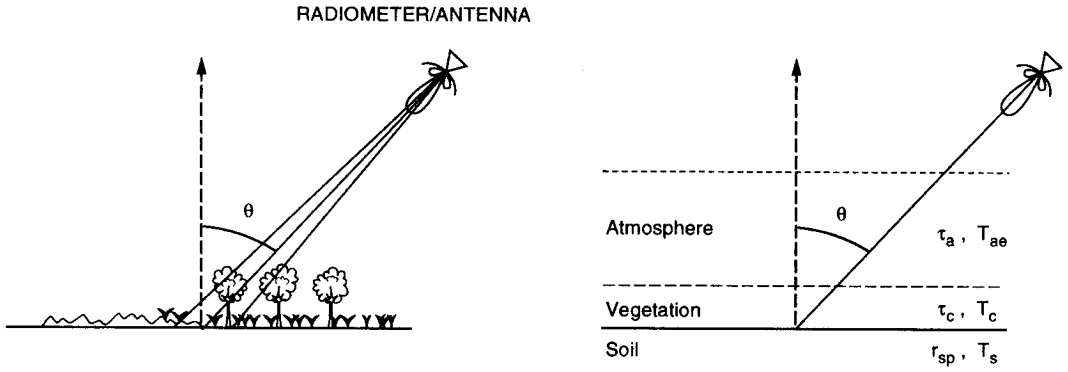

Figure 4: Model Representation of a Spaceborne Radiometer Viewing A Heterogeneous Earth Surface

$$T_{B_p} = T_u + \exp(-\tau_a)\left[\{ T_d\, r_{s_p} \exp(-2\tau_c) \} + \right.$$
$$\left. + \{ e_{s_p}\, T_s \exp(-\tau_c) + T_c\,(1 - \omega_p)\,[\,1 - \exp(-\tau_c)\,]\,[\,1 + r_{s_p} \exp(-\tau_c)\,] \} \right] \qquad (1)$$

where, T_u is the upwelling atmospheric emission, T_d is the downwelling atmospheric and space-background emission at the top of the vegetation, and τ_a is the atmospheric opacity. The subscript p denotes either vertical or horizontal polarization. T_c is the vegetation temperature, τ_c is the vegetation opacity, r_{s_p} is the soil reflectivity (related to the soil emissivity e_{s_p} by $e_{s_p} = 1 - r_{s_p}$), and T_s is the effective soil temperature (the effective temperature is the weighted-average temperature over the microwave penetration depth in the medium). The vegetation single scattering albedo is given by ω_p. The derivation of Equation (1) assumes a specular soil surface with no reflection at the air-vegetation boundary. This expression has been found to be a good approximation up to ~10 GHz for a vegetation layer overlying a rough soil surface provided r_{s_p} is interpreted as the rough soil surface reflectivity.

A simplifying approximation is that the vegetation and underlying soil are at close to the same physical temperature T_e. This approximation does not degrade the moisture retrieval accuracy, but will result in the retrieval of a mean or 'effective' radiating temperature of the composite soil/vegetation medium. (It is difficult to retrieve T_s and T_c independently in any case except where the vegetation and soil characteristics are well known a-priori. Substituting $T_s \cong T_c = T_e$ in Equation (1) we obtain:

$$T_{B_p} = T_u + \exp(-\tau_a)\left[\{ T_d\, r_{s_p} \exp(-2\tau_c) \} + \right.$$
$$\left. + T_e \{ (1 - r_{s_p}) \exp(-\tau_c) + (1 - \omega_p)\,[\,1 - \exp(-\tau_c)\,]\,[\,1 + r_{s_p} \exp(-\tau_c)\,] \} \right] \qquad (2)$$

The expression in the second curly brackets is the effective emissivity of the soil/vegetation surface.

Atmosphere

Standard expressions for T_u and T_d can be obtained from the literature (e.g. Hofer and Njoku, 1981). At atmospheric window frequencies T_u and T_d can be expressed using the effective radiating temperature approximation as (ignoring the space contribution to T_d:

$$T_u \cong T_d \cong T_{ae} [1 - \exp(-\tau_a)] \tag{3}$$

where, T_{ae} is the mean temperature of the microwave-emitting region of the atmosphere. The expression is valid for most atmospheric water vapor and cloud conditions. T_{ae} is frequency dependent and depends also on the vertical distributions of temperature, humidity, and liquid water. Up to 37 GHz, however, the dependence of T_{ae} on atmospheric profile variability is small, and T_{ae} may be expressed simply as a function of the surface air temperature T_{as} and a frequency-dependent offset δT_a:

$$T_{ae} \cong T_{as} - \delta T_a \tag{4}$$

The effect of uncertainty in T_{ae} on the observed T_{B_p} is actually sufficiently small that climatological values suffice for T_{as}, δT_a, and hence T_{ae}.

The opacity τ_a along the atmospheric path is dependent on the viewing angle θ and the precipitable water q_v and vertical-column cloud liquid water q_l. It can be expressed (for a plane parallel atmosphere) as:

$$\tau_a = (\tau_o + a_v\, q_v + a_l\, q_l) / \cos\theta \tag{5}$$

where, τ_o is the oxygen opacity at nadir, and a_v and a_l are frequency-dependent coefficients. Values for these coefficients are derived from standard expressions for water vapor and droplet absorption in the atmosphere (Rayleigh absorption is assumed for the cloud droplets).

Surface

The dependence of τ_c on vegetation columnar water content w_e follows an approximately linear relationship which may be written as:

$$\tau_c = b\, w_e / \cos\theta \tag{6}$$

where, $\cos\theta$ accounts for the slant path through the vegetation. The coefficient b depends on canopy structure and frequency. Theory and experimental data suggest that for a given vegetation type b is approximately proportional to frequency at frequencies below ~10 GHz (Jackson and Schmugge, 1991; Wegmuller et al., 1995; LeVine and Karam, 1996). These studies indicate,

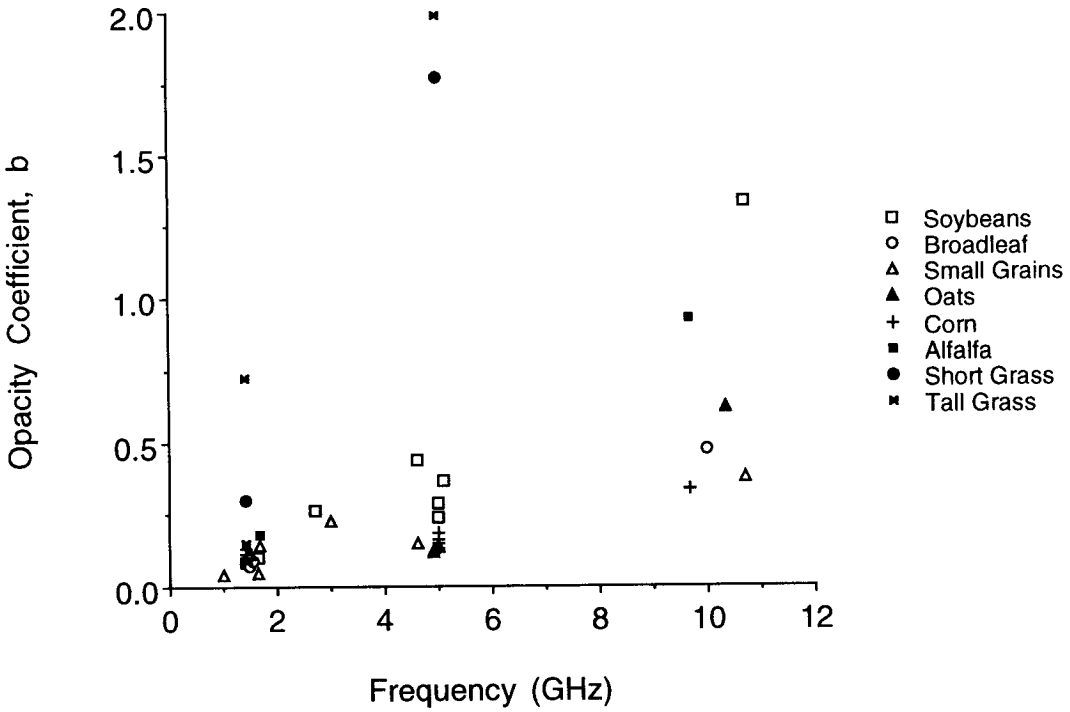

Figure 5: Dependence of vegetation opacity coefficient b on frequency for different vegetation types (adapted from Jackson and Schmugge, 1991).

however, that at higher frequencies the frequency dependence of b decreases, and its dependence on canopy structure increases. This provides rationale for restricting the physically-based retrieval algorithm to the use of 6.9 and 10.7 GHz. Figure 5 shows experimentally derived values of b as a function of frequency, for some specific vegetation types (from Jackson and Schmugge, 1991).

The reflectivity of rough soil, r_{s_p}, is related to that of smooth soil, r_{o_p}, by the semi-empirical formulation (Wang and Choudhury, 1981; Wang et al., 1983):

$$r_{s_v} = [\,(1 - Q)\, r_{o_v} + Q\, r_{o_h}\,] \exp(-h) \tag{7}$$

$$r_{s_h} = [\,(1 - Q)\, r_{o_h} + Q\, r_{o_v}\,] \exp(-h) \tag{8}$$

The form of the above expressions is suggested by scattering theory of randomly rough surfaces, according to which the reflectivity r_{s_p} can be decomposed into coherent and incoherent parts (Tsang and Newton, 1982). The exponential term in the expressions is derived from the coherent part, where h is related to the surface height standard deviation σ. The terms in brackets describe mixing of the co- and cross-polarized scattered radiation, where the parameter Q is related to both h and the horizontal correlation length l. This formulation does not represent the detailed surface roughness characteristics found in nature. However, measurements at the AMSR footprint scale will average over terrain of many types, which suggests that the averaged effect of roughness on

microwave brightness can be represented adequately using the above formulation. Values for the parameters h and Q must be obtained empirically. Initial values will be used which will be fine-tuned as part of the algorithm calibration procedure. For a given location the roughness parameters are not expected to exhibit significant temporal variability at the AMSR footrpint scale.

The Fresnel expressions relate the reflectivities r_{o_v} and r_{o_h} of a smooth, homogeneous soil to the complex dielectric constant of the soil ε_r:

$$r_{o_v} = \left| \frac{\varepsilon_r \cos\theta - \sqrt{\varepsilon_r - \sin^2\theta}}{\varepsilon_r \cos\theta + \sqrt{\varepsilon_r - \sin^2\theta}} \right|^2 \tag{9}$$

$$r_{o_h} = \left| \frac{\cos\theta - \sqrt{\varepsilon_r - \sin^2\theta}}{\cos\theta + \sqrt{\varepsilon_r - \sin^2\theta}} \right|^2 \tag{10}$$

where, θ is the incidence angle relative to the surface normal. For a given frequency, the dielectric constant depends on the volumetric soil moisture content m_e and to a lesser extent on soil type. (There is also a small dependence on soil temperature.) This relationship can be expressed as:

$$\varepsilon_r = f(m_e\,;\, \rho_b, s, c) \tag{11}$$

To compute ε_r the soil is considered as a mixture of soil particles and pore spaces filled with air and water (Wang and Schmugge, 1980; Dobson et al., 1985). The Dobson et al. model requires specification of the sand and clay mass fractions s and c (which describe the soil texture) and the soil bulk density ρ_b. Figure 6 illustrates the dependence of emissivity on soil moisture at 6.9 and 10.7 GHz for smooth soils, as derived from the dielectric model. The high sensitivity of brightness temperature to soil moisture (~3 K/% volumetric soil moisture for a soil temperature of 300 K) is the principal advantage of using microwave radiometry for soil moisture sensing.

Model Summary

Equations (2)–(11) summarize the dependence of observed brightness temperature on the land surface and atmosphere geophysical variables. The model equations can be represented as:

$$T_{B_i} = \Phi_i(\mathbf{x}) \tag{12}$$

where, the model function $\Phi_i(\mathbf{x})$ relates the brightness temperature observations T_{B_i} at channel i to the parameters $\mathbf{x} = \{x_j\}$ of the soil-vegetation-atmosphere medium.

The model parameters are listed in Table 4. The parameters are grouped in two categories: (a) parameters defining sensor and media characteristics that are constant or vary slowly with time, and (b) media geophysical variables. Atmospheric variables are included for completeness, although the sensitivity of brightness temperature to these variables (over land) is too low for

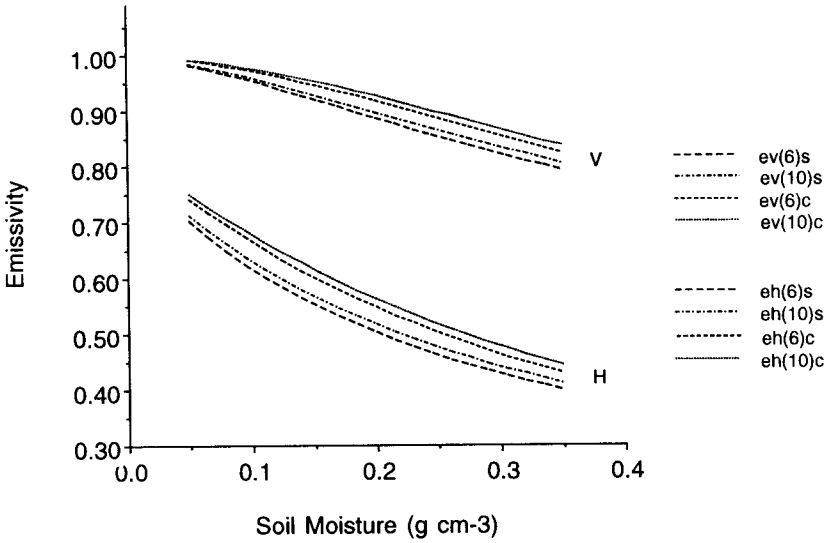

Figure 6: Dependence of emissivity on soil moisture for a smooth soil at 6 and 10 GHz, V and H polarization, and for sand (s) and clay (c) type soils.

reliable retrievals. (Retrieval of water vapor may be possible over surfaces with low emissivity variability.) In the retrieval algorithm, the atmospheric variables and media characteristics are given fixed values derived from ancillary databases or climatology (Section 3.1.2). The parameterization represented by Table 4 is a reasonable compromise between complexity and accuracy for the ~70-km-scale AMSR retrievals.

Effects of Inhomogeneity

The model described above does not consider nonuniform moisture and temperature profiles in the soil, or heterogeneity of surface types and characteristics within a footprint. The model is a valid representation, however, provided the parameters m_e, T_e, and w_e are considered as spatial averages over the horizontal footprint and vertical sampling depth in the medium.

Vertically Nonuniform Profiles

For nonuniform temperature and moisture profiles, the dependence of soil brightness temperature T_{bs_p} on the subsurface temperature profile $T_s(z)$ and moisture profile $m(z)$ can be expressed as:

$$T_{bs_p} = \int_{-\infty}^{0} T_s(z)\, F_p\{\varepsilon_r(z)\}\, dz \tag{13}$$

where, z is the vertical dimension (positive in the upward direction), and $\varepsilon_r(z)$ is the complex

Table 4: Parameters of the Microwave Model

Parameter	Description
(a) Media & Sensor Parameters	
Atmosphere:	
τ_o	Oxygen nadir opacity
a_v, a_l	Water vapor and liquid water opacity coefficients
δT_a	Lapse rate temperature differential (K)
Vegetation:	
ω_p	Single scattering albedo
b	Opacity coefficient
Soil:	
h, Q	Roughness coefficients
ρ_b	Bulk density (g cm^{-3})
s, c	Sand and clay mass fractions
Sensor:	
θ	Viewing angle (deg)
ν	Frequency (GHz)
p	Polarization
(b) Media Variables	
Atmosphere:	
q_v	Precipitable water (cm)
q_l	Cloud liquid water path (mm)
T_{as}	Surface air temperature (K)
Land Surface:	
m_e	Surface soil moisture (g cm^{-3})
w_e	Vegetation water content (kg m^{-2})
T_e	Surface temperature (K)

dielectric constant profile which depends on $m(z)$. The form of $F_p\{\varepsilon_r(z)\}$ can be determined by modeling the electromagnetic propagation in inhomogeneous media (Njoku and Kong, 1977). An approximate form for $F_p\{\varepsilon_r(z)\}$, valid when the moisture profile does not vary rapidly over the depth of a wavelength in the medium (the wavelength in the medium varies with dielectric constant and hence also with depth), can be determined using an incoherent radiative transfer approach which leads to expressions equivalent to (13):

$$T_{bs_p} = (1 - r_{s_p})\, T_e \tag{14}$$

$$T_e = \int_{-\infty}^{0} T_s(z)\, \widetilde{F}_{N_p}\{\varepsilon_r(z)\}\, dz \tag{15}$$

where, r_{s_p} now denotes the reflectivity of a homogeneous soil of dielectric constant $\varepsilon_r(0)$, (i.e. $\varepsilon_r(z)$ at $z = 0$), T_e is the soil 'effective temperature', and $\widetilde{F}_{N_p}\{\varepsilon_r(z)\}$ is an approximation of $F_p\{\varepsilon_r(z)\}$ normalized to an integral of unity:

$$\widetilde{F}_{N_p}\{\varepsilon_r(z)\} = \alpha(z) \exp\left(- \int_z^0 \alpha(z')\, dz' \right) \tag{16}$$

$$\alpha(z) = 2\, Im\left\{ \frac{2\pi}{\lambda} \sqrt{\varepsilon_r(z) - \sin^2\theta} \right\} \tag{17}$$

Equations (14)–(17) show that, to first order, the reflectivity (and emissivity) is determined by the dielectric constant (and hence the soil moisture) at the surface ($z = 0$), while the brightness temperature is affected by the subsurface temperature and moisture profiles. As the wavelength increases, the approximation becomes less accurate since the emissivity is affected by the subsurface dielectric constant gradient as well as the surface value. The approximation is still useful, however, provided that the emissivity is considered to be representative of the average moisture m_e within a top soil layer of depth d_m, the 'moisture sensing depth', where d_m depends on wavelength. Simulations have shown (e.g. Wilheit, 1978) that d_m is about a tenth of a wavelength in the medium. Thus, d_m is a variable that is dependent on the surface soil moisture content. The longest AMSR wavelength is 4.3 cm, and for a dry soil the wavelength in the medium is about half this value. Thus, we find for AMSR that $d_m < 2$ mm. The AMSR soil moisture retrieval is therefore a 'skin surface' value.

Figure 7 shows the weighting functions $\widetilde{F}_{N_p}\{\varepsilon_r(z)\}$ for two representative moisture profiles. The bulk of the soil emission comes from the neighborhood around the maxima of the weighting functions, which may occur significantly below the surface for some profiles. For uniform soil moisture (i.e. uniform dielectric constant), and nadir-viewing, $\widetilde{F}_{N_p}\{\varepsilon_r(z)\}$ takes the simple form:

$$\widetilde{F}_{N_p}\{\varepsilon_r(z)\} = \alpha \exp(\alpha z) \tag{18}$$

$$\alpha = \frac{4\pi n''}{\lambda} \tag{19}$$

where n'' is the imaginary part of the refractive index (square root of the dielectric constant), i.e. $n'' = Im\{\sqrt{\varepsilon_r}\}$. The 'temperature sensing depth' $d_t = \alpha^{-1}$ is defined as the depth of the surface layer from which ~63% of the emitted radiation originates. Alternatively, d_t is the distance in the medium over which the intensity of transmitted radiation decreases by a factor of $e^{-1} = 0.368$ (for a medium of uniform temperature and moisture). d_t is also often referred to as the 'penetration depth' in the medium. Figure 8 shows the dependence of d_t on frequency and soil moisture for a sandy soil.

In summary, for inhomogeneous moisture and temperature profiles, m_e is interpreted as the mean soil moisture over the depth d_m, and T_e is the mean soil temperature over the depth d_t.

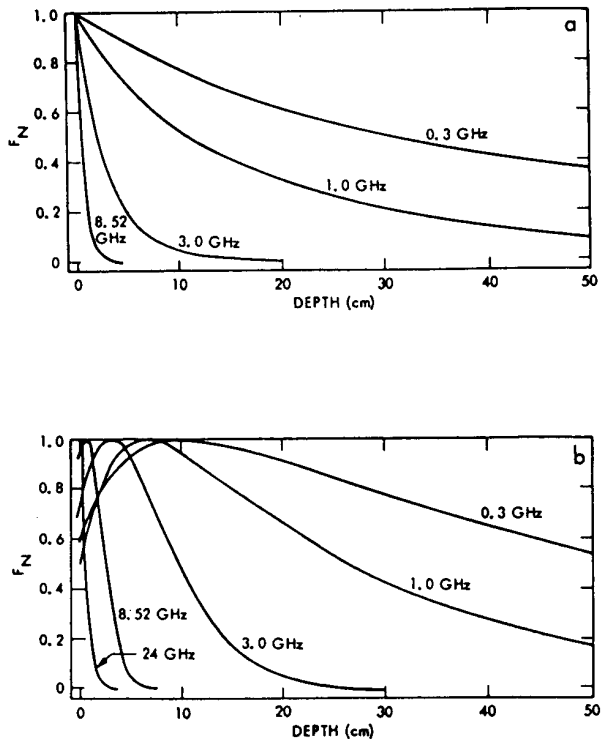

Figure 7: Normalized temperature weighting functions for: (a) wet moisture profile, (b) profile with dry surface and rapidly increasing moisture with depth.

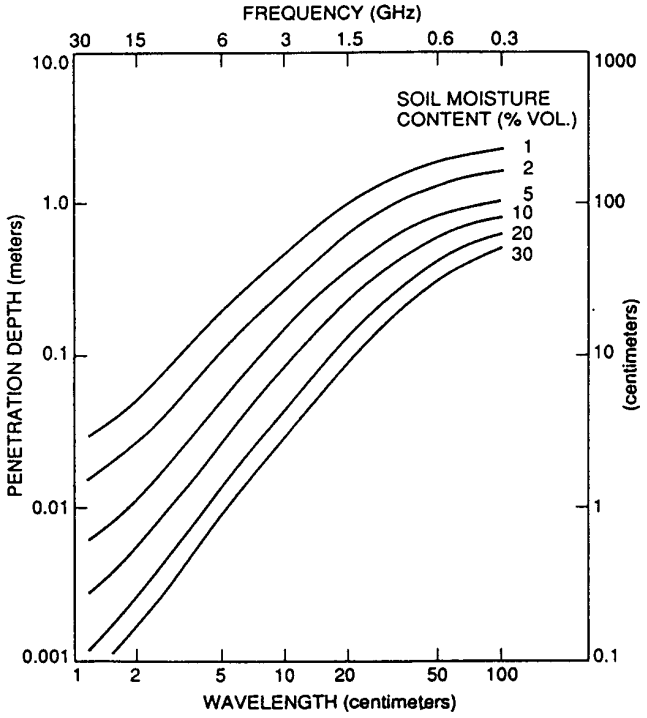

Figure 8: Microwave soil penetration depth as a function of frequency and moisture content

Horizontal Heterogeneity:

For a heterogeneous scene (Figure 4), the parameters and terms of Equation (2) represent area-averages within the observed footprint. The horizontal footprint and area-weighting are defined by the antenna pattern.

If we consider a simple representation, in which the antenna pattern is uniform within the footprint area, and zero outside, then the observed brightness temperature T_b will be an area-average of the component brightness temperatures T_{b_j} within the footprint, i.e.

$$T_b = \sum_{j=1}^{N} f_j T_{b_j} \tag{20}$$

where, f_j are the fractional coverages of N distinct surface types within the footprint (the f_j sum to unity). A simplified analysis (Njoku et al., 1995b) shows that estimates of area-averaged geophysical variables (surface temperature T_e,vegetation water content w_e, and soil moisture m_e), retrieved from the area-averaged brightnesses T_b, will be related to the component variables by the following equations:

$$T_e = \frac{1}{e} \sum_{j=1}^{N} f_j e_j T_{e_j} \tag{21}$$

$$w_e = - \frac{\cos\theta}{b} \ln \left\{ \sum_{j=1}^{N} f_j \exp [-b w_{e_j} / \cos\theta] \right\} \tag{22}$$

$$m_e = \frac{\sum_{j=1}^{N} f_j m_{e_j} \exp [-b w_{e_j} / \cos\theta]}{\exp [-b w_e / \cos\theta]} \tag{23}$$

$$e = \sum_{j=1}^{N} f_j e_j \tag{24}$$

The effects of nonlinearity caused by the presence of vegetation are evident. We may define 'composite' parameters x' (where x may refer to T_e, w_e, or m_e) as those obtained by a direct area-averaging of the geophysical variables over the footprint, i.e.

$$x' = \sum_{j=1}^{N} f_j x_j \tag{25}$$

We can then examine the differences $\Delta x = x - x'$ between variables retrieved from area-averaged brightnesses (Equations (21)–(23)) and those obtained by area-averaging the component variables (Equation (25)). Simulations of Δx have been carried out for a variety of two-component surfaces (Njoku et al., 1995b). Figure 9 shows the results for soil moisture Δm_e. The effects of

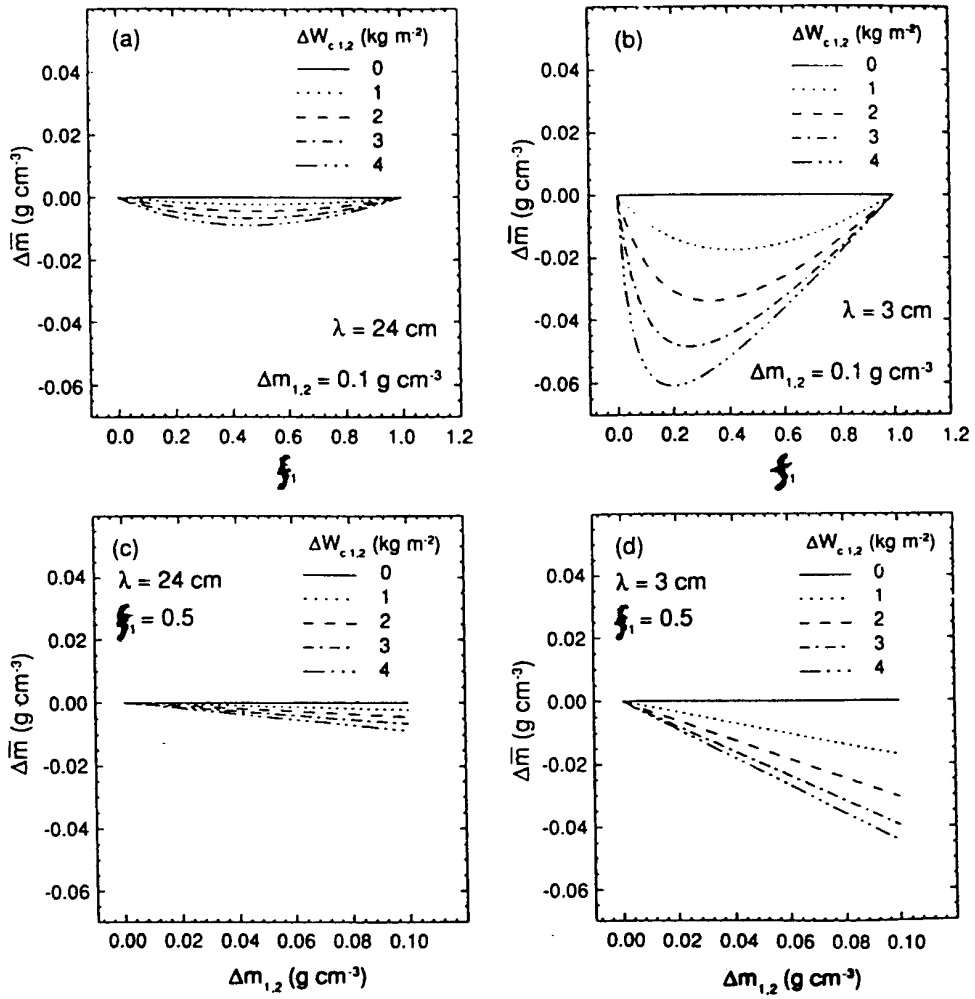

Figure 8: Difference $\Delta m = m - m'$ (see text) for a two-component surface: (a) as a function of fractional cover f_1 for soil moisture contrast $\Delta m_{1,2}$ = 0.1 g cm^{-3}, with vegetation water content contrast $\Delta W_{c1,2}$ as a parameter, at a wavelength of 24 cm; (b) same as (a) but for a wavelength of 3 cm; (c) as a function of soil moisture contrast $\Delta m_{1,2}$ with vegetation water content contrast $\Delta W_{c1,2}$ as a parameter, for fractional cover f_1 = 0.5, at a wavelength of 24 cm; (d) same as (c) but for a wavelength of 3 cm. (Njoku et al., 1995b).

nonlinearity are small except in situations where roughly equal fractions of bare soil and dense vegetation occur within the footprint. Such cases must be considered carefully when interpreting the AMSR land retrievals.

Model Calibration

Uncertainty in the absolute calibration of the AMSR brightness temperatures and in some of the model parameters requires that the retrieval model first be 'calibrated' to the AMSR observations. This will be done by selecting homogeneous sites, e.g. deserts and tropical forests, where offsets in the brightness temperatures at the various channels can be determined, and the model parameters h, Q, and ω_p can be fine-tuned. Since the roughness characteristics of desert, and the single scattering albedo of tropical forest, are not expected to change significantly with time, the parameters h, Q, and ω_p are determined once, and then held constant in the temporal application of the algorithm. As AMSR data continue to be acquired over monthly and seasonal time scales, the spatial (and any temporal) dependence of these parameters can be studied to improve the algorithm performance.

Desert

Over the desert site, with an assumption of no vegetation ($\tau_c \rightarrow 0$), the model equations can be rearranged to express the soil reflectivity as a function of the observed brightness temperature, surface temperature, and atmospheric absorption and emission:

$$r_{s_p} = \frac{T_{B_p} - T_u - T_e \exp(-\tau_a)}{\exp(-\tau_a)\left\{ T_d - T_e + T_{sky} \exp(-\tau_a) \right\}} \tag{26}$$

Estimates of q_v, T_{ae}, and T_e from forecast model output, and AMSR brightness temperatures, will be used to evaluate r_{s_h} and r_{s_v} at desert sites (with cloud filtering if necessary) according to Equation (26). Values for h and Q will be obtained for each frequency.

Forest

Over the forest site, the high vegetation opacity masks the underlying soil. Using the limit $\tau_c \rightarrow$ large, we can rearrange the model equations to express the vegetation single-scattering albedo as a function of the observed brightness temperature, surface temperature, and atmospheric absorption and emission:

$$\omega_p = 1 - \frac{(T_{B_p} - T_u)}{T_e \exp(-\tau_a)} \tag{27}$$

Using forecast model output and AMSR data over the forest sites, as for the desert sites, values for ω_p will obtained at each frequency and polarization.

By matching the model to the AMSR observations at the calibration sites we lump any residual brightness temperature calibration offsets into the derived values of h, Q, and ω_p. It is difficult to distinguish absolute radiometric calibration offsets from model offsets without more extensive analysis. This will be done on a continuing basis throughout the mission.

Sensitivities

The sensitivity S_{ij} of brightness temperature at channel i to geophysical parameter x_j can be expressed as:

$$S_{ij} = \left| X_j \left(\frac{\partial \Phi_i}{\partial x_j} \right)_{\mathbf{x} = \mathbf{x}_o} \right| \tag{28}$$

where, X_j are typical geophysical parameter dynamic ranges and $\mathbf{x}_o$ are baseline values of the parameters $\mathbf{x}$ at which the sensitivities are evaluated. Normalizing the sensitivities by the ranges X_j indicates more clearly the relative magnitudes of the sensitivities to the different variables in Kelvins. Table 5 shows the computed sensitivities for horizontal and vertical polarizations at 6.9 GHz. Two cases are shown, one for a baseline of bare soil and one for a baseline vegetation water content of 1.5 kg m^{-2} (spanning the range of vegetation conditions under which we believe soil moisture retrievals will be feasible). The sensitivity to moisture and vegetation are clearly much reduced at the higher vegetation level, although good sensitivity remains to surface temperature. The sensitivity differences between H and V polarizations, and between frequencies (10.6 GHz not shown), enable the four-channel retrieval algorithm to discriminate between the moisture, vegetation, and temperature variables. Sensitivities to other variable and model parameters are typically an order of magnitude or so less than to the three main variables (soil moisture, surface temperature, and vegetation water content), and hence are not dominant factors in the retrievals.

3.1.2 Mathematical Description of the Algorithm

Retrievals of land surface parameters have in the past used principally surface classification and linear-regression methods (e.g. McFarland et al., 1990; Jackson and LeVine, 1996). Nonlinear algorithms (iterative and neural-network based) have also been studied (Zurk et al., 1992; Njoku et al., 1994) particularly to improve retrievals where the physics of the radiative transfer and interaction processes are nonlinear. Bayesian estimation techniques have been investigated to include, optimally, a-priori information on sensor noise, model uncertainties, probability distributions of the parameters being estimated, and ancillary data from ground truth or other sensors (Davis et al., 1995). The baseline AMSR algorithm is a nonlinear, iterative algorithm, and is a compromise from the viewpoints of physical basis, global applicability, and maturity. As discussed earlier, the retrievals will be performed at the 6.9 GHz footprint resolution since the 6.9 GHz frequency is essential to the soil moisture retrieval. The effects of subpixel heterogeneity are expected to be small except for special cases. These effects will be studied in a research mode, but retrievals at higher spatial resolution will not be part of the baseline algorithm.

Table 5(a): Normalized sensitivities at 6.6 GHz, H and V polarizations, and θ = 50°, for given parameter ranges X_j and baseline values x_{oj}. Vegetation baseline is w_e = 0 kg m^{-2} (bare soil).

Parameter	Range (X_j)	Baseline (x_{oj})	Sensitivity, H S_{ij} (K)	Sensitivity, V S_{ij} (K)
Soil moisture, m_e (g cm^{-3})	0.32	0.15	95.5	60.1
Surface temperature, T_e (°C)	40	20	25.1	35.7
Vegetation water, w_e (kg m^{-2})	1.5	0	211.3	28.1
Precipitable water, q_v (cm)	5	2.5	1.3	0.18

Table 5(b): As for Table 5(a), except vegetation baseline is w_e = 1.5 kg m^{-2}.

Parameter	Range (X_j)	Baseline (x_{oj})	Sensitivity, H S_{ij} (K)	Sensitivity, V S_{ij} (K)
Soil moisture, m_e (g cm^{-3})	0.32	0.15	8.5	5.3
Surface temperature, T_e (°C)	40	20	22.0	20.6
Vegetation water, w_e (kg m^{-2})	1.5	1.5	10.9	1.2
Precipitable water, q_v (cm)	5	2.5	0.12	0.02

Baseline Algorithm

The algorithm retrieves simultaneously the three primary variables m_e, w_e, and T_e, from measurements at four channels (6.9 and 10.7 GHz, V and H polarization; i = 1 to 4). The algorithm is based on the radiative transfer model Φ_i (**x**) (Equation (12)). The definitions of the retrieved variables are:

- m_e : Surface soil moisture (g cm^{-3})—the soil moisture in the top few millimeters of soil, averaged over the retrieval footprint.
- w_e : Vegetation water content (kg m^{-2})—the water content in the vertical column of vegetation overlying the soil, averaged over the retrieval footprint.
- T_e : Land-surface temperature (K)—the microwave radiating temperature of the surface, averaged over the retrieval footprint.

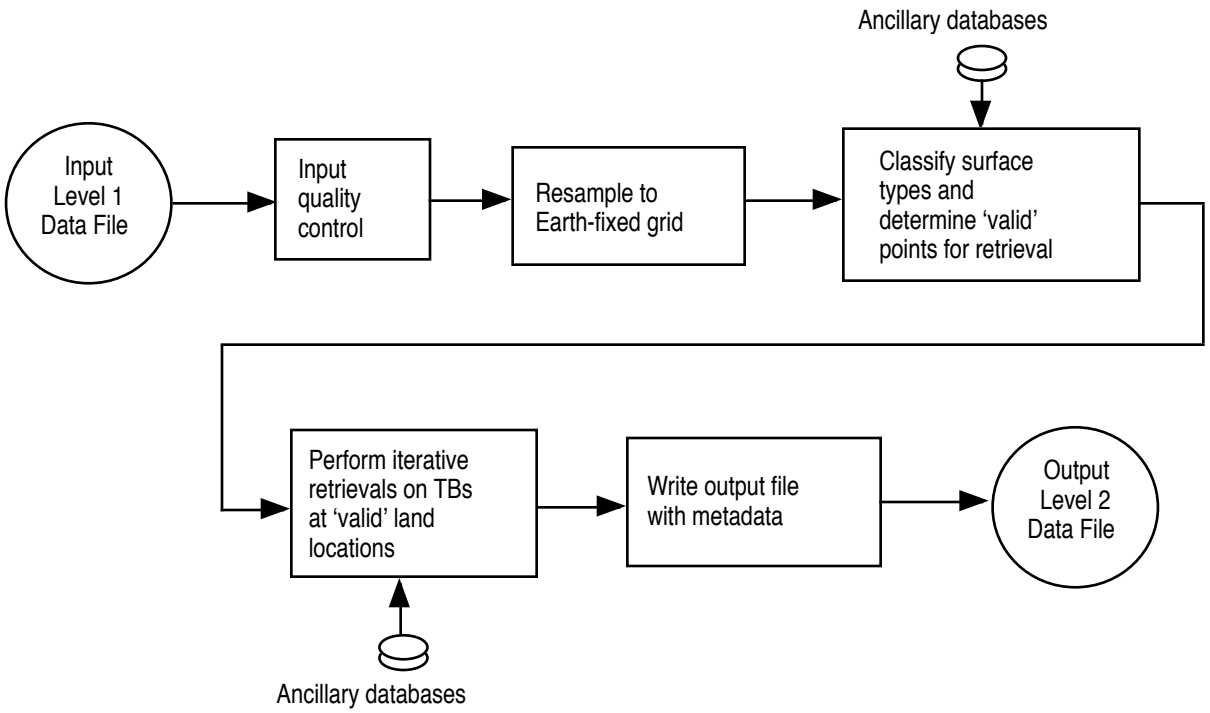

Figure 10: Land algorithm flowchart

The algorithm flowchart is shown in Figure 10. The AMSR brightness temperatures (T_bs) are first resampled (for a given swath) to an Earth-fixed grid. The gridded T_bs are then classified to determine feasible points for retrieval. Gridding facilitates combination of the T_bs with ancillary data for the classification and retrieval steps, and also allows statistics of T_bs and retrieved parameters to be accumulated at fixed grid locations from successive orbits. The loss in retrieval accuracy caused by gridding the T_bs prior to geophysical retrieval is small compared to other uncertainties. The retrieved parameters are output as gridded level 2 products (no averaging over multiple orbits is done).

Resampling to Earth Grid

The NSIDC EASE-Grid is considered as the baseline grid for the AMSR land retrievals. The EASE-Grid was developed by the National Snow and Ice Data Center (NSIDC) for gridding SSM/I data products. The version to be used is the global, cylindrical, equal-area projection, with a nominal grid spacing of approximately 25 x 25 km (true at 30°N&S). The size of the grid is 1383 columns x 586 rows. A description of the EASE-Grid can be found at the NSIDC URL http://www-nsidc.colorado.edu/NASA/GUIDE/EASE/. Alternatively, a rectangular latitude-longitude grid can be used, with a spacing of 0.25° x 0.25° and size of 1440 x 720. However, this

is not an equal-area grid. The advantage of an equal-area grid is that the resampling statistics at each grid point are characteristic of the same number of input data points. The grid used is referred to below as the AMSR land grid. The swath brightness temperatures will be resampled to the AMSR land grid using either a 'drop-in-the-bucket' or 'distance-weighting' method. The drop-in-the-bucket method is simplest—all data samples that fall within a grid cell are averaged together. However, the distance-weighting method may introduce less interpolation error.

Ancillary Databases

Four types of databases will be used in the surface classification and retrievals. The purpose of the databases is to identify valid grid points for retrieval and to aid in the geophysical retrieval. The databases will be obtained from archived sources and pre-processed to the AMSR land grid.

Surface Topography—will be derived from the U.S. Geological Survey EROS Data Center GTOPO30 global digital elevation model. The horizontal grid spacing is 30 arc seconds. Pre-processing of these data will enable screening out points over ocean, mountainous terrain, and where the topographic variation within a grid cell is likely to degrade the geophysical retrievals.

Soil Texture (sand and clay fraction)—will be derived from a 1°x1° lat-lon global soil type database (Webb et al., 1992) for use in estimation of soil dielectric properties as a function of soil moisture content. Higher resolution databases are available for use in certain regions (e.g. U.S.).

Vegetation Type—will be derived from the USGS EDC 1 km global land cover characteristics database. These data will be used in estimating the dependence on vegetation type of the model coefficient b relating vegetation water content to vegetation opacity.

Atmospheric Parameters (precipitable water and surface air temperature)—will be derived from the NCEP or ECMWF global reanalysis datasets (climatology) or the real-time forecast model outputs. These data will be used for estimating atmospheric contributions in the geophysical retrieval algorithm.

Surface Type Classification

The surface type classification is done to identify and screen (prior to retrieval) grid cells that include major water bodies, mountainous regions, dense vegetation, snow, frozen ground, and precipitation, for which retrievals will not be possible. All other grid points are considered 'valid' for retrieval. The databases described above will be used to classify permanent features. The AMSR snow and precipitation algorithms (developed by other AMSR investigators) will be used to classify variable snow cover and precipitation.

Retrieval

In the iterative procedure, the values of the geophysical parameters to be retrieved $\mathbf{x} = \{m_e, w_e,$ and $T_e\}$ are adjusted to minimize the weighted-sum of squared differences χ^2 between observed, $T_{B_i}^{obs}$, and computed, $\Phi_i(\mathbf{x})$, brightness temperatures. The Levenberg-Marquardt algorithm is used for the minimization (Press et al., 1989).

$$\chi^2 = \sum_{i=1}^{4} \left(\frac{T_{B_i}^{obs} - \Phi_i(\mathbf{x})}{\sigma_i} \right)^2 \qquad (29)$$

At each retrieval point, the algorithm starts with a-priori values of the geophysical variables $\mathbf{x_o}$ and adjusts these iteratively until convergence to the χ^2 minimum is achieved. σ_i represents the measurement noise in channel i. The model Φ_i ($\mathbf{x}$) is mathematically well-behaved, hence convergence is normally fast, except where the model cannot adequately represent the surface emission (e.g. where snow or open water occur in the footprint), or where the sensitivity to the parameters is too low. This occurs, for example, in the retrieval of m_e and w_e in densely-vegetated areas. In such cases the retrievals are unreliable, as indicated by high values of the minimized χ^2. The atmospheric variables of the model—q_v, q_l, T_{as}, and δT_a—are given a-priori values derived from climatology. The atmospheric parameters τ_o, a_v, and a_w, are known constants. The parameters b, h, Q, ω_p, ρ_b, s, and c are given fixed values based on the model calibration and ancillary data discussed in the previous section, and will be fine-tuned after launch to calibrate the model using AMSR observations at designated calibration sites.

Enhanced Algorithms

Bayesian estimation will be investigated for implementing constraints on the retrievals in a formal way—by incorporating a-priori statistics (joint probability distributions) of the surface and atmospheric characteristics and the brightness temperatures themselves. Information will be obtained from ancillary databases and the time-history of AMSR brightness temperatures. The a-priori distribution covariances relative to the sensor and model mismatch covariances will be adjusted in order to ensure stable and well-behaved retrievals. The a-priori covariances will be poorly known at the start of the AMSR mission. However, as the database of global brightness temperatures and retrievals is built up after launch the algorithm will 'learn' by multi-temporal analysis and become more optimal in utilizing the improved a-priori knowledge. Algorithms to propagate the remotely sensed surface information to greater depths in the soil, e.g. using a heat- and water-flux soil model, will also be investigated in collaboration with EOS IDS investigators, following the approaches of Entekhabi et al (1994) and others.

3.1.3 Variance and Uncertainty Estimates

Estimates of the retrieval uncertainties of the baseline algorithm have been obtained by simulation studies and by tests using Nimbus-7 SMMR data.

Simulation Studies

In the simulation studies the variables to be estimated, $\mathbf{x} = \{m_e, w_e, T_e\}$, were simulated as sets of uniform random variables spanning the dynamic ranges: $m_e = 0.03$ to 0.35 g cm^{-3}; $w_e = 0$ to 1.5 kg m^{-2}; $T_e = 0$ to 40 °C; and $q_v = 1$ to 5 cm. From these distributions, the brightness temperatures $T_{B_i} = \Phi_i(\mathbf{x})$ were computed at six SMMR channels used in the retrieval (6.6, 10.7, and 18 GHz; V and H polarizations). (Six channels were used in the simulation study, but the 18

GHz channels were found to provide little additional information.) Gaussian random noise of 0.3 K (1σ) was added to simulate the SMMR observations $T_{B_i}^{obs}$*. The retrieval algorithm was applied to the simulated observations, and parameter estimates **x*** were obtained. The uncertainty estimates in the retrieval procedure were then obtained from the means and standard deviations of the errors $\varepsilon = \mathbf{x}^* - \mathbf{x}$.

The results are shown in Figure 11. Panels (a) through (d) show the soil moisture retrieval error means and standard deviations as functions of m_e, w_e, T_e, and q_v respectively. Similarly, panels (e) through (h), (i) through (l), and (m) through (p) show the retrieval errors for vegetation water content, surface temperature, and precipitable water. The solid lines are the means, and the dashed lines the standard deviations, of the errors. In general, the mean errors are all close to zero indicating that the retrievals are unbiased over the full ranges of variability. The slight wiggliness of the lines is the statistical uncertainty in the simulation of estimating the mean errors using n_r = 200 realizations. The retrieval error standard deviations are not very sensitive to T_e and q_v, except for ε_q which has a broad peak with a maximum near T_e = 14 C. Within the surface temperature range corresponding to this peak, for the conditions of our simulation, the background surface brightness temperature is similar to the tropospheric water vapor emitting temperature, and hence there is little sensitivity of the satellite-observed brightness temperature to the water vapor. This points out the difficulty of retrieving water vapor (or cloud liquid water) over land, except where the land brightness temperature is much lower, or higher than the tropospheric water vapor (or cloud) emitting temperature.

A significant feature of Figure 11 is the increase in error standard deviations ε_m and ε_w with increase in vegetation water content (panels (b) and (f)). This is expected, due to the masking of the underlying soil and the saturation of vegetation emission at the higher vegetation amounts, at frequencies of 6.6 GHz and above. There is little potential for using the SMMR (or AMSR) for retrieval of m_e or w_e at values of w_e > ~1.5 kg m^{-2}. At vegetation amounts below ~0.2 kg m^{-2} (approaching bare soil) the surface temperature retrieval error, ε_T, increases markedly (panel (j). For bare soils, the algorithm has difficulty discriminating between the effects on brightness temperature of increasing T_e and decreasing m_e (note the corresponding increase in ε_m in panel (b)). This implies that for bare soils the soil moisture retrievals may benefit from the use of ancillary surface temperature data from other sources (satellite or in situ), if available with sufficient accuracy.

Tests Using SMMR Data

The simulation results (Figure 11) indicate that, accounting for modeling errors (which we have not simulated here), retrieval accuracies for m_e, w_e,and T_e of better than 0.06 g cm^{-3}, 0.1 kg m^{-2}, and 2.5 C, respectively, should be feasible using satellite instruments such as the SMMR and AMSR over a wide range of conditions, provided the footprint-averaged vegetation water content is less than about 1.5 kg m^{-2}. No externally provided data are assumed. The model used in the simulations does not account for surface heterogeneity, variability in surface topography and roughness, or uncertainties in model parameters. Thus, it is important to test the retrieval

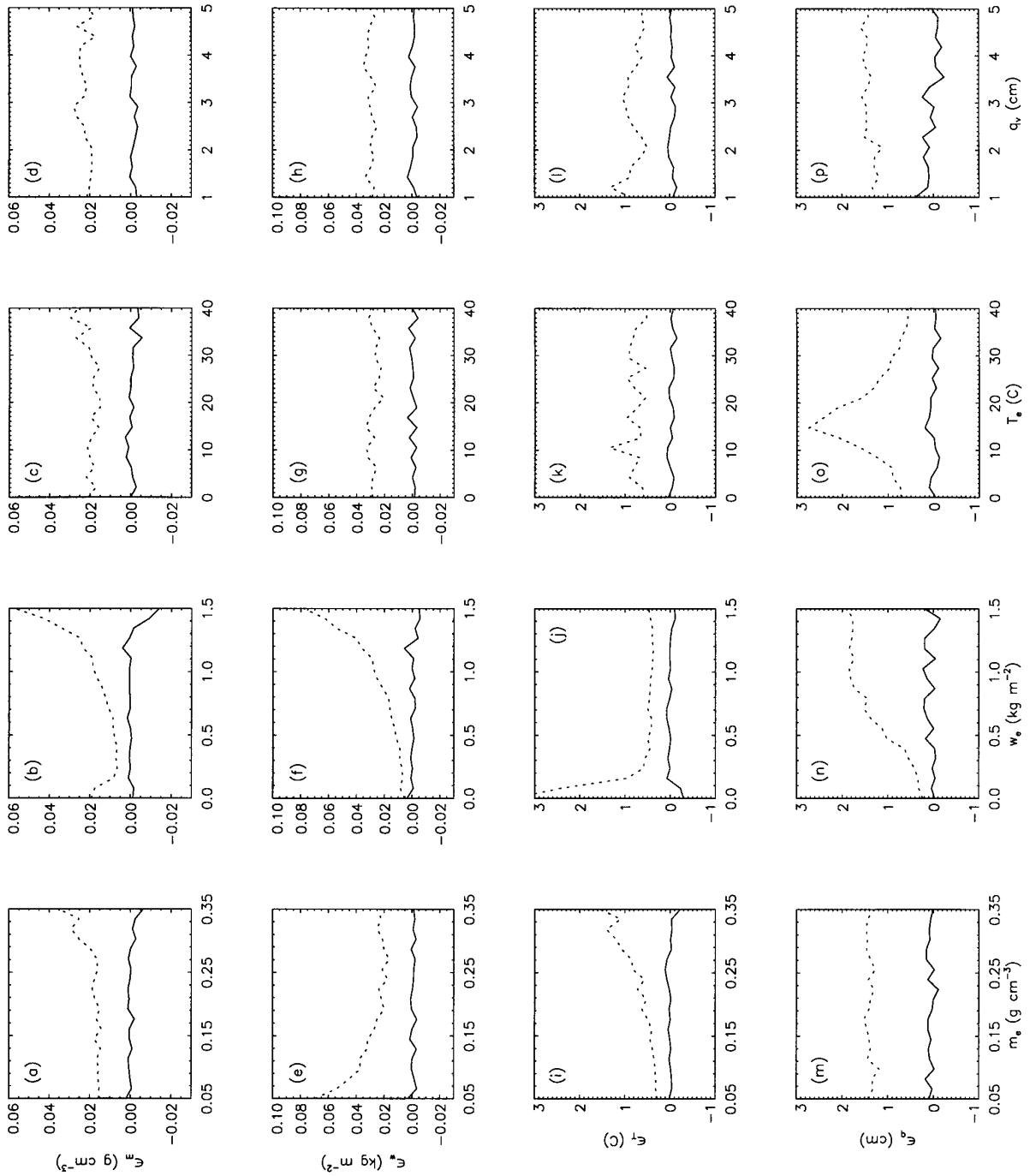

Figure 11: Simulated retrievals using Nimbus-7 SMMR characteristics (see text for details).

algorithm using actual satellite data, under conditions in which the performance can be readily assessed. We have tested the algorithm using four years of Nimbus-7 SMMR data over a 4° x 10° latitude-longitude region of the African Sahel, between 12° to 16°N, and 0° to 10°E. In this region there are strong seasonal signals of moisture, vegetation, and temperature, related to the rainy and dry seasons. The region is devoid of large-scale topography, and the surface can be viewed as relatively homogeneous at the large scale of the SMMR footprints. The region is a fragile ecosystem, and hence is also of interest due to the threat of drought and desertification.

The SMMR data were derived from the reprocessed SMMR brightness temperature data set available from the NSIDC DAAC. The data were binned separately for daytime and nighttime passes (ascending and descending orbits, respectively) onto 6-day and monthly 1/2° x 1/2° lat-lon grids for ease of data handling and comparison with other data sets. The retrieval algorithm was applied to the monthly, daytime binned data; thus the geophysical parameter estimates are also at the monthly 1/2° grid scale. Daytime data were used since there are extensive gaps in the SMMR nighttime data near the equator due to the alternate-day on-off operation of the sensor (the on-off switching was done at the descending-node equator crossing near local midnight).

Figure 12(a) shows a time-series of the SMMR-derived geophysical parameters, retrieved on the 1/2° grid, and further averaged over the Sahel study region. Superimposed on the plot is the precipitation rate, averaged over the same region, obtained from an operational forecast model product of the National Centers for Environmental Prediction (NCEP). Figure 12(b) shows comparisons between the SMMR retrievals of m_e and T_e and the NCEP model outputs of soil wetness and surface temperature. The variables in Figure 12 have been scaled as indicated, to have similar dynamic ranges on the plots. The NCEP model output products are part of a 13-year (1982-94) operational forecast model reanalysis project. The products are generated as outputs of a 6-hourly data-assimilation and forecast cycle, and the products shown here were obtained from NCEP as monthly-averages on a 2.5° x 2.5° grid, and then averaged over the study area. The model output data cannot be considered as 'truth' but they represent self-consistency in the forecast model as related to the in-situ data used in the most recent (6-hourly) data assimilation. Thus, the data are valuable for comparing against the temporal trends of the SMMR retrievals.

Figure 12(b) demonstrates the ability to retrieve soil moisture and temperature from the SMMR with the correct seasonal cycle. It is difficult to compare quantitatively the absolute values of the SMMR retrievals and the NCEP data, since the NCEP soil wetness represents an average value over the top 10 cm, as compared to the top few mm for the SMMR. Thus, the SMMR derived values of soil moisture are more than a factor of four lower than the NCEP values. Also, the NCEP surface temperature is a skin surface value, as compared to the top few cm for the SMMR. In addition, the SMMR data are samples near 12 noon local time, while the NCEP data are averages over the diurnal cycle. It is interesting to note the dip in the SMMR-retrieved surface temperatures (Figure 12(a)) that appear to coincide with the peaks of the NCEP rain estimates. These dips are less pronounced in the NCEP temperatures (Figure 12(b)), but are visible as plateaus on the decreasing side of the curves. Normally, under moist conditions the soil temperature is cooler than for a dry soil, due to the increased evaporation from the soil and the soil thermal inertia. This cooling effect is more pronounced in the SMMR data sampled near local noon than for the diurnally-averaged NCEP data.

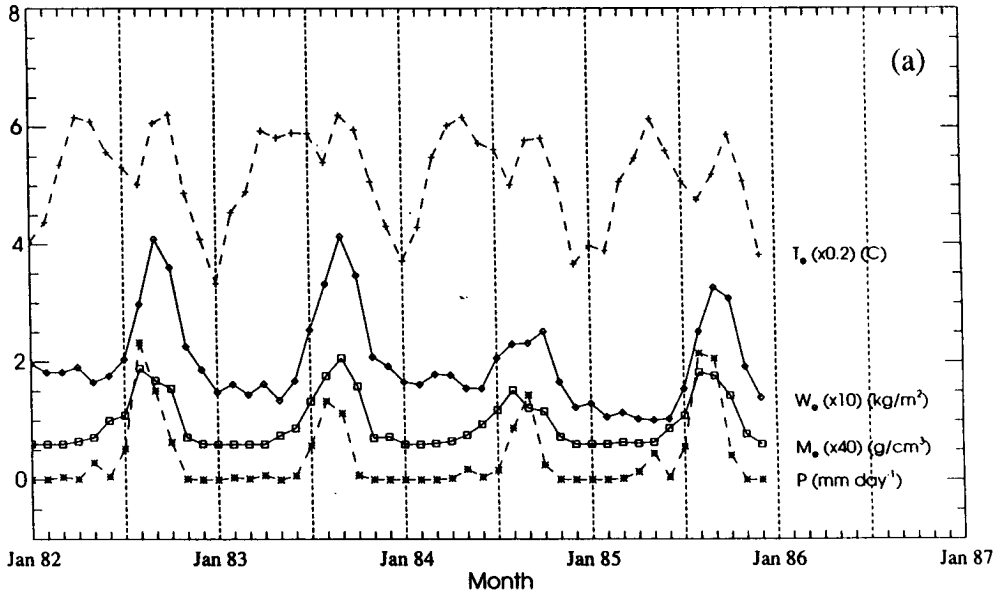

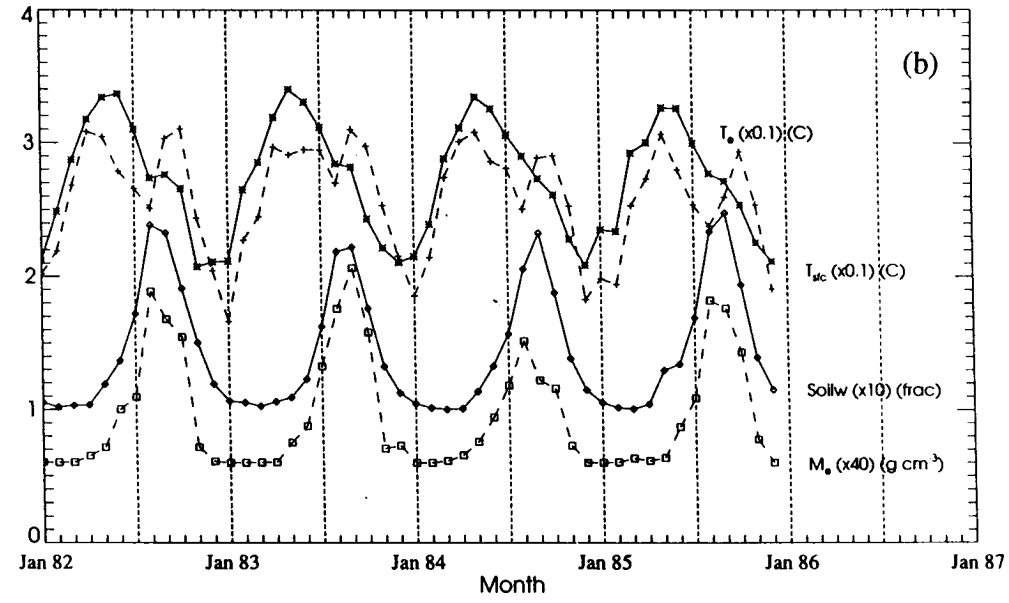

Figure 12: Monthly time-series of geophysical parameters retrieved from Nimbus SMMR data in the Sahelian zone, and comparisons with model output data from the NCEP reanalysis (see text for discussion).

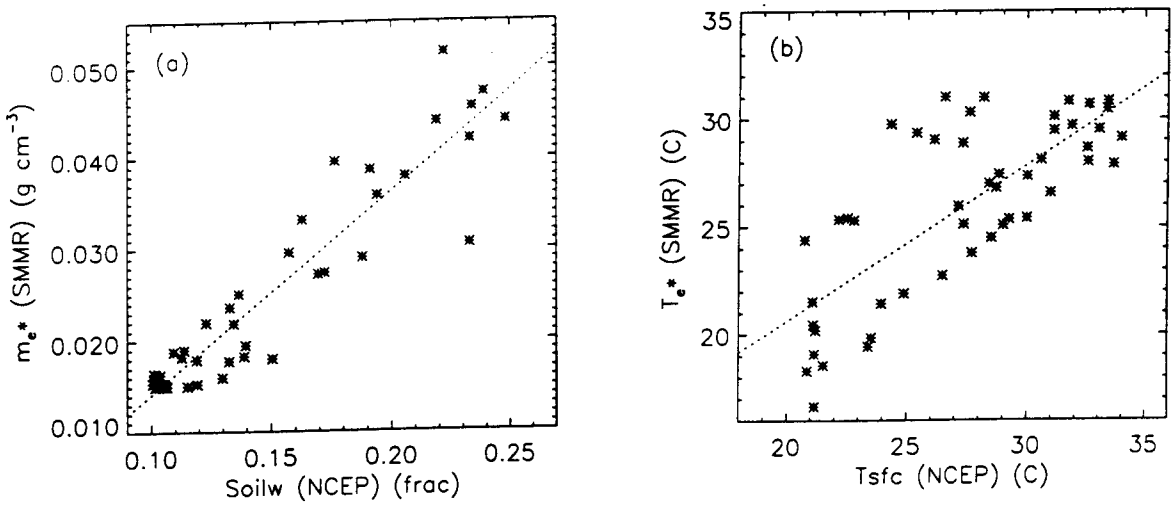

Figure 13: Scatterplots of SMMR-derived versus NCEP reanalysis variables shown in Figure 12.

Figure 13 shows scatterplots of the SMMR-derived and NCEP model output variables shown in Figure 12(b). The best fit regression lines are also shown. The standard deviation of the temperature comparisons in Figure 13(b) is 2.7 C. Different quantities are being compared between the remotely-sensed and model output data, and the data represent monthly averages, over a relatively large 4° x 10° area. Nevertheless, the level of agreement is good. Better agreement is to be expected when the comparisons can be carried out at shorter time scales, such that the moisture and temperature variations can be tracked more accurately, and where the accuracy of the comparison data can be better verified. The Sahel is a region where the accuracy of the operational forecast models is suspect, due to the sparseness of in situ meteorological data for initializing the forecasts.

3.2 PRACTICAL CONSIDERATIONS

3.2.1 Numerical Computation Considerations

The baseline algorithm has been tested using Nimbus-7 SMMR data with similar channels to AMSR, i.e. 6.6 and 10.7 GHz, V and H polarizations. The main computational burden is the iterative retrieval at each grid point which requires computing the forward model at each iteration. This can be speeded up by using approximations to the radiative transfer equations. Since the overall AMSR data rate is relatively low compared with other EOS sensors, the AMSR land algorithm is not expected to be a major driver for the EOSDIS processing system. There are no special-purpose hardware or software requirements.

3.2.2 Programming/Procedural Considerations

To determine 'valid' points for the land retrievals the algorithm uses static ancillary databases and simple threshholding classification of the brightness temperatures. Information from the AMSR snow cover and precipitation over land algorithms (see the individual ATBDs for these

algorithms) may be used also. The combined size of the ancillary databases is estimated as approximately 20 Mbytes. MODIS data will be used on an experimental basis (research mode) to examine sub-pixel heterogeneity effects. Further discussion of these items and the algorithm flowchart is given in Section 3.1.2. Algorithms will be written in FORTRAN-77 with portability to run on UNIX-based platforms. Data products will be structured and formatted according to EOSDIS guidelines. Coordination will be maintained with the appropriate EOSDIS DAAC in providing documentation, algorithms, and data appropriate for archival and public distribution.

3.2.3 Calibration and Validation

Validation can be performed either directly on parameters derived from AMSR observations or in conjunction with data assimilation methods and integrated hydrometeorological models. Validation should include intercomparisons of similar data products developed by different instruments and models. Validation will be performed in collaboration with end users of the AMSR land products (investigators of hydrologic process studies, climate monitoring, and data assimilation) to ensure that the uncertainties and associated statistics meet their requirements.

Model Calibration

Model calibration has been discussed in Section 3.1.1. The procedure involves estimating the radiometric calibration offsets and fine-tuning the parameterization of the microwave model. It will be performed initially during the 2-month period immediately after launch, making use of globally-distributed calibration regions, reasonably homogeneous over the footprint scale, that can be characterized by a small number of parameters. These regions include deserts, savannas, grasslands, and dry and humid forest regions. Surface truth data, including surface air-temperature, humidity, precipitation, surface moisture, and biomass from measurement programs at many of these sites, will be used. Model parameter values of single scattering albedo over forests, and surface roughness coefficients over deserts, will be verified in this manner. The algorithm calibration analysis will be performed at intervals during the mission to fine-tune the calibration if necessary. Figure 14 shows the locations of candidate calibration sites, and Table 6 lists their attributes.

Validation Issues

Validation of the AMSR land products will begin after the initial algorithm calibration period. The objective of the validation will be to esimate the actual (as opposed to simulated) errors and their space-time variabilities. Validation will thus be a continuing process throughout the lifetime of the AMSR mission. The following are expected to be the major sources of uncertainty in the output products:

- Footprints may contain mixtures of different surface types, hence the retrievals represent area-averaged parameters over the ~70-km footprints. In cases where there are large contrasts (heterogeneity) within the footprint the retrieved quantities may not represent accurate area-averages due to nonlinearities in the radiative transfer processes. (It is assumed that area-averages are appropriate for hydrologic and climate models.)

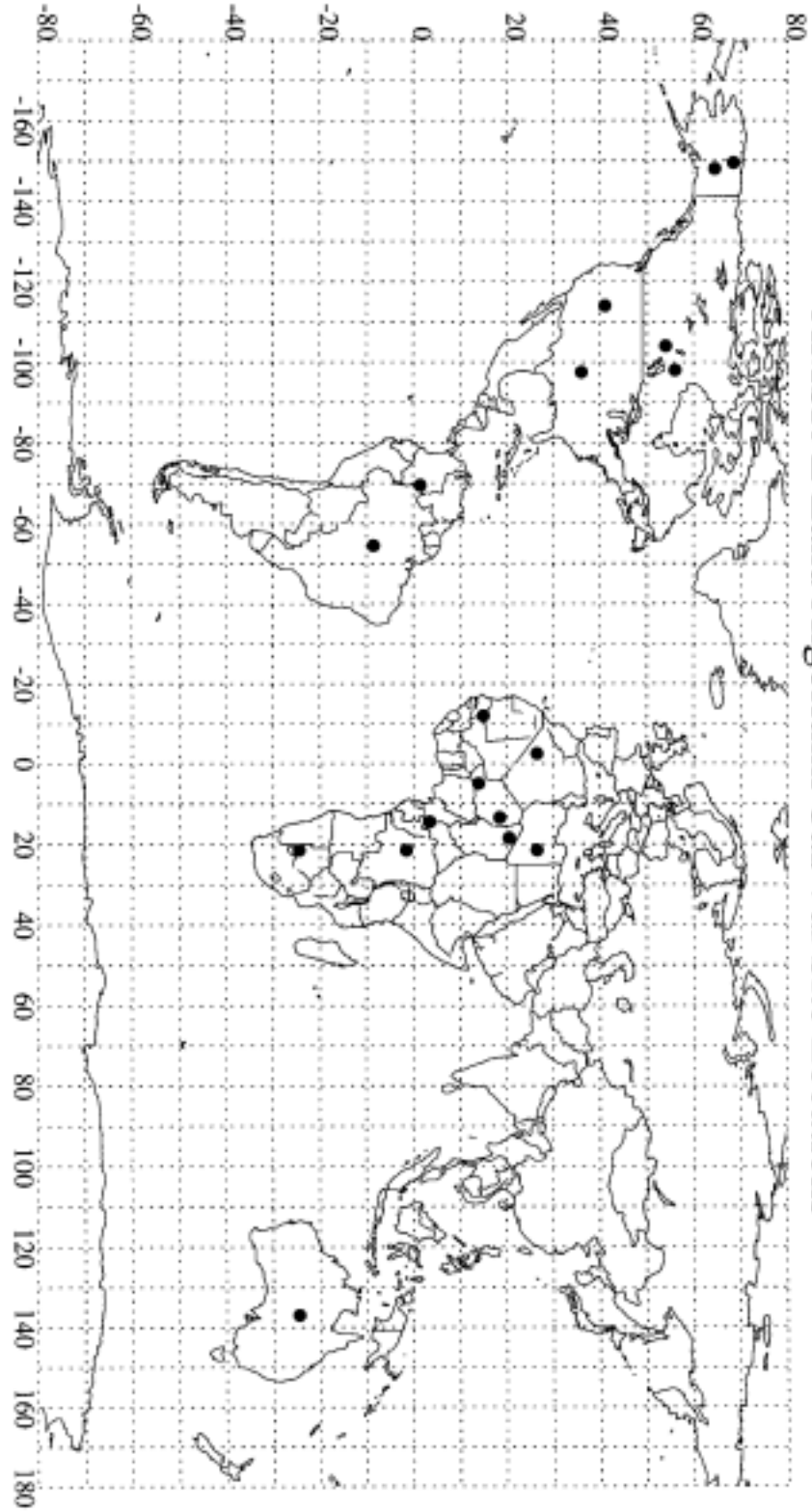
AMSR-E Land Algorithm Cal/Val Site Locations
80
60
40
20
0
-20
-40
-60
-80
-160 -140 -120 -100 -80 -60 -40 -20 0 20 40 60 80 100 120 140 160 180

Figure 14

Table 6: AMSR Land Algorithm Calibration Analysis Sites

#	Ecosystem	Name	Region	Lat-Lon	Attributes
1	Desert	Simpson Desert	Central Australia	23.5-25.5 S 136-138 E	Low Relief, S. Hemisphere
2	Desert	Kalahari Desert	S.W. Botswana	23-26 S 20-23 E	Low Relief, S. Hemisphere
3	Desert	Western Desert	W. Egypt	25-28 N 25-28 E	Low Relief, N. Hemisphere
4	Desert	Sebkha Mekerrhane	S. Central Algeria	25-28 N 1-4 W	Moderate Relief, N. Hemisphere
5	Desert	Tibesti Mountains	N.W Chad	19-22 N 17-20 E	High Relief, N. Hemisphere
6	Sahel	Bilma	E. Niger	17-20 N 12-15 E	Northern Sahel
7	Sahel	Tahoua	S.W. Niger	13-15 N 4-6 E	Central Sahel
8	Sahel	Kayes	Mali/Senegal	14-16 N 11-13 W	Western Sahel
9	Tropical Forest	Boumba	S.E. Cameroon	2-5 N 13-16 E	Africa, N. Hemisphere
10	Tropical Forest	Salonga	Central Zaire	0-3 S 20-23 E	Africa, S. Hemisphere
11	Tropical Forest	Mitu	Colombia/ Brazil	0-3 N 68-71 W	S. America N. Hemisphere
12	Tropical Forest	Curua	Central Brazil	7-10 S 53-56 W	S. America, S. Hemisphere
13	Boreal Forest	Boreas SSA	Saskatchewan, Canada	53.5-54.5 N 103.5-104.5 W	Southern BOREAS Experiment Site
14	Boreal Forest	Boreas NSA	Manitoba, Canada	55.5-56.5 N 97.5-98.5 W	Northern BOREAS Experoment Site
15	Boreal Forest	Bonanza Creek	Central Alaska, U.S.	64-65 N 147.5-148.5 W	Ecological Forest Experimental Site
16	Tundra	Toolic Lake	N. Central Alaska, U.S.	68-69 N 149-150 W	LTER Site
17	Salt Lake Basin	Great Salt Lake	N.W. Utah, U.S.	38-44 N 111-117 W	Desert Hydrologic Basin
18	Plains Grassland	Southern Great Plains	Oklahoma/ Kansas, U.S.	34-38 N 96-99 W	Subhumid Hydrologic Basin

- The retrieved variables represent averages over the microwave vertical sampling depth in the medium. This depth varies according to the amount of moisture in the soil and/or vegetation. The different sampling depths at 6.9 and 10.6 GHz may give rise to some ambiguity in the retrievals where the moisture and temperature profiles are highly nonuniform.

- The retrieval errors for m_e and w_e will increase with vegetation cover. The vegetation threshholds for reliability of the retrievals can only roughly be estimated at this time. Additional pre-launch simulations and experience with AMSR data during the validation phase may help establish these threshholds more precisely.

- Uncertainties associated with radiative transfer model parameters (such as soil roughness, vegetation scattering and opacity coefficients, soil texture, etc.) will propagate into the retrieval uncertainties for m_e, w_e, and T_e.

A major validation challenge is the large AMSR footprint scale (~70 km). Considerable resources (beyond the capability of a single investigation) are required to mount an in situ measurement campaign that can adequately characterize spatial fields of soil moisture, temperature, and biomass at such scales within the time frame of a satellite overpass. Reasonable estimates of spatial fields can be obtained, however, by assimilation of distributed in situ point measurements into hydrologic models, and by comparison with remotely sensed data from other satellite instruments. The AMSR land validation activities will therefore be performed in collaboration with other modeling efforts and field programs, augmenting these where feasible for this investigation. The following issues are pertinent:

- A small number of test sites are needed to characterize the spatial variability of soil moisture, surface temperature and vegetation over the AMSR footprint scale during short-term intensive field measurement and modeling campaigns. Two or more sites in different climate regimes are desirable. Validation at these sites will be referred to as 'Type 1' validation.

- Other sites are needed, less intensively sampled, that can provide a continuous source of measurements from operational in situ networks. Assimilation of these data into land surface models will provide validation fields of lower spatial resolution but over larger regions and continuous in time. Validation against these fields will be referred to as 'Type 2' validation.

- For both types of validation, model output data are needed such as from the International Global Soil Wetness Project, the operational forecast centers (NCEP and ECMWF), the NASA/GSFC Data Assimilation Office, or other specialized modeling efforts that can participate in this study.

- Sources of in situ data to be used in the validations will include:

    - Established observation programs, including the Oklahoma Mesonet, DOE Atmospheric Radiation Measurement (ARM) Program, NSF Long-Term Ecological Research (LTER) sites, and the WCRP Baseline Surface Radiation Network (BSRN)

- In-situ measurements from the former Soviet Union, China, and State of Illinois
- Field experiments carried out under the WCRP and IGBP. These include GEWEX Regional Continental Scale Experiments: GCIP (in the U.S. Mississippi Basin), GAME (in the Asian Monsoon regions), and LBA (in the Amazon Basin).
- Surface-based observations obtained by EOS interdisciplinary and other instrument investigations

Validation Sites and Methodology

Soil moisture is the primary AMSR-derived parameter to be validated in the Type 1 validation experiments. Soil moisture and surface temperature will be validated against the model assimilation outputs in the Type 2 validations. Vegetation water content will be validated primarily by comparisons with products from other remote sensors, such as Leaf Area Index from MODIS. The use of other remotely sensed data at higher spatial resolution than AMSR, e.g SAR, MODIS, AIRS, will provide additional comparative validation for the AMSR soil moisture and temperature retrievals, and will assist in determining the effects of spatial heterogeneity within the AMSR footprint.

The principal Type 1 field validation site will be in the U.S. Southern Great Plains (SGP) centered in Oklahoma (Figure 15). This site covers a region of approximately 500 x 300 km, and is perhaps the best instrumented site for surface soil moisture, hydrology, and meteorology in the world. The region has major East-West precipitation gradients which result in a large range of seasonal soil moisture. The vegetation cover also has a significant range. The region includes several major observation networks and research field sites (Oklahoma Mesonet, ARM-CART, ARS Micronet), and is part of the GEWEX-GCIP focus study area. The site was the location of the SGP'97 experiment in July 1997, in which a comprehensive set of soil moisture, surface characteristics, and boundary-layer flux measurements were acquired (organized as part of an EOS interdisciplinary investigation - T. Jackson, PI), using a variety of in situ and remote sensing instruments. Table 7 provides a list of potential data sources for generation of future validation data sets for this region.

Three AMSR-dedicated SGP field experiments are planned in 1999, 2001, and perhaps 2003 as follow-ons to the SGP'97 experiment, assuming Aqua and ADEOS-II launches in December 2000 and November 2001, respectively. The first experiment will provide a database for AMSR algorithm fine-tuning and as a reference for assessing interannual change with the preceding and subsequent experiments. The second and third experiments will provide data for post-launch validation of the AMSR land products from Aqua and ADEOS-II. Soil moisture validation products will be created from the field experiment data, containing fused multi-sensor observations. Observations at different spatial and temporal scales will be merged to form statistically optimal estimates of the validation data set state variables (soil moisture and soil temperature in the 0 to -5 cm and -5 to -15, and -15 to -25 cm depths, and vegetation leaf area index and dry and moist weight; both on 3 km x 3 km gridding). Weights based on the error structure of different sources of observations will be used to form a single estimate of the state variables. This is an ambitious strategy and will rely on resources and funding support from cooperative programs and projects.

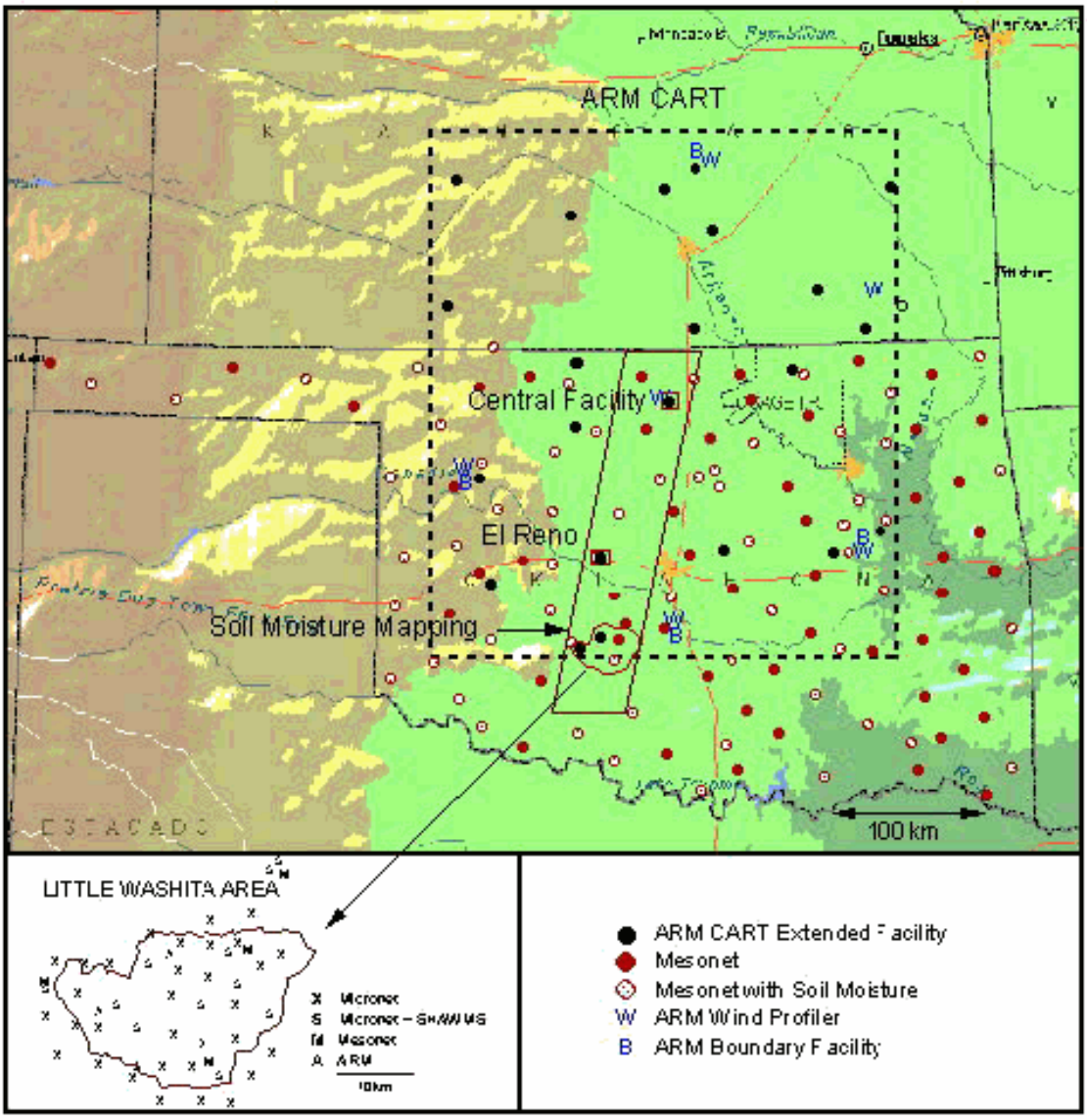

Figure 15: The principal Type 1 field validation site in the U.S. Southern Great Plains (SGP) centered in Oklahoma. (Figure provided by T. Jackson, USDA/ARS Hydrology Lab, Beltsville, MD.)

The 1999 SGP experiment (SGP99) has been carried out as planned in July 1999. The experiment was conducted successfully using several airborne radiometers and extensive ground-based instrumentation and soil moisture, temperature, and vegetation sampling. A complete description of the experiment plan and data are provided at the SGP99 web site http://hydrolab.arsusda.gov/sgp99/. Other Type 1 validation sites are presently under consideration that will take advantage of cooperative experiments with international programs

Table 7: Characteristics and sources of observations for soil moisture validation data set development at the SGP field site.

Physical Parameter	Spatial Resolution	Temporal Frequency	Source
Surface air Micrometeorology	One Station per 10^3 km^2	15 Minutes	Oklahoma Mesonet
Soil Temperature	One Station per 10^3 km^2	15 Minutes	Oklahoma Mesonet
Soil Matric Head	One Station per 10^3 km^2	15 Minutes Capaticance Probes	Oklahoma Mesonet
Area-Average Precipitation	4 km x 4 km	Hourly	NWS ABRFC
Volumetric Soil Moisture	Variable	Episodic along Flight Lines	NWS NOHRSC Aircraft Instrument (Gamma-Radiation)
Vegetation Parameters	10 km x 10 km 30 km x 30 km	Daily Weekly	Vis/IR Polar-Orbiting (MODIS) & VIS/IR Geostationary (GOES-8) satellites
Volumetric Soil Moisture	30 km x 30 km	12 Hourly	NCEP NWP Initialization
Soil Temperature	30 km x 30 km	12 Hourly	NCEP NWP Initialization
Near Surface Air Parameters	30 km x 30 km	12 Hourly	NCEP NWP Initialization
Volumetric Soil Moisture	Point	Episodic	Gravimetric Measurements
Volumetric Soil Moisture	0.5 km x 0.5 km	Episodic	Aicraft remote sensing

including the Japanese ADEOS-II project, EOS instrument teams (AIRS and MODIS), and EOS interdisciplinary investigations.

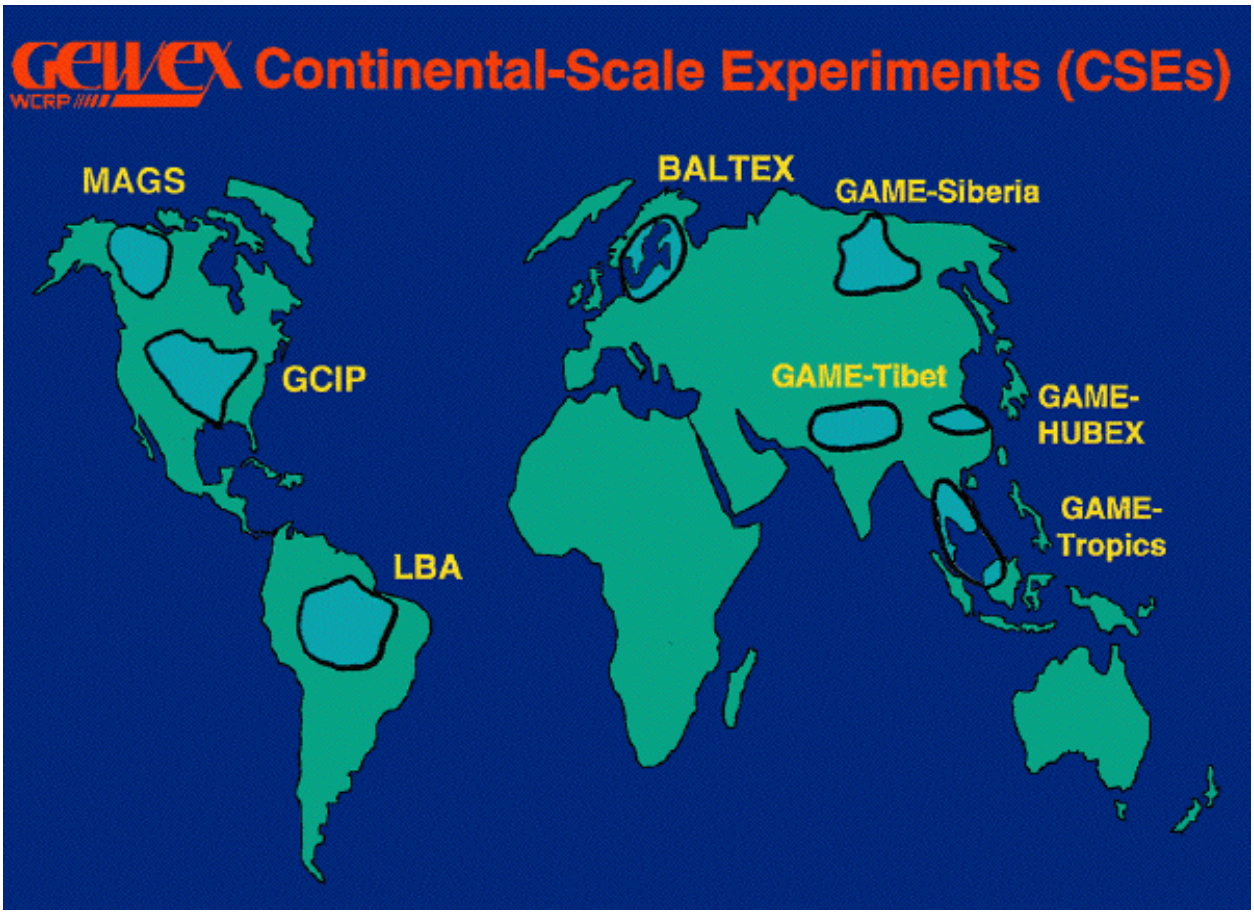

Figure 16: Location of the GEWEX Regional Continental-Scale Experiments. GCIP, GAME, and LBA will be the main sites of interest for AMSR validation.

Type 2 validation sites will involve primarily the GEWEX Regional Continental Scale Experiments (RCEs) including GCIP, GAME, and LBA (Figure 16). The RCEs deploy long-term hydrometeorological monitoring networks that will provide distributed surface observations spanning a continuous period through the AMSR mission. Special field experiments as well as continuing four-dimensional data assimilation (4DDA) and macroscale hydrological modeling will be conducted under these programs. Participation and data sharing arrangements will be negotiated with these programs. For example, GCIP is currently providing a 5-year documentation of aspects of hydrologic-atmosphere coupling across the U.S., and will leave in place an ongoing observational framework against which soil moisture comparisons can be made. These data include distributed fields of rainfall from gauges and NEXRAD rain-radar systems, runoff, modeled evaporation, analyzed fields of temperature and humidity, and, at certain locations, arrays of sensors to provide direct measurements of soil moisture. Augmentation of these arrays is being planned within a 200x200 km study area in Oklahoma and Kansas as part of the Atmospheric Radiation Measurement (ARM) Project, and could be extended elsewhere in the Mississippi River basin. These arrays will be valuable as direct sources of comparison data for AMSR over selected

regions of the U.S., but can serve also to validate model-based soil moisture estimates for the U.S. as a whole, which will then be compared with AMSR soil moisture fields.

Global Scale Validation

Validation on a global scale is difficult since the only independent sources are products derived from global atmospheric models, calculated using the soil hydrology from the budgets of energy and water at the Earth's surface. Key parameters, such as precipitation and the surface net radiation, depend on the parameterizations used within the models, and their errors are often hard to assess. Forecast centers routinely perform data assimilation experiments with and without specific satellite products. From these, the regional and global output error fields of critical near-surface parameters can be examined regionally and globally, such as the 2-m temperature and humidity that are measured in-situ, and are closely linked to soil moisture initialization. The forecast errors resulting from using different soil moisture initializations (model or satellite derived for example) will be examined to assess the impact on the forecast accuracy of the satellite derived soil moisture in comparison with the purely model derived product. These studies will be pursued in collaboration with the GSFC Data Assimilation Office, and the operational forecast centers (NCEP and ECMWF), and will rely on their support to perform the assimilation studies.

Joint Aqua-ADEOS-II AMSR Validation Plans

Plans are being made to use validation sites in the Asian region, principally Mongolia and Tibet, that are being considered as primary validation sites for soil moisture products to be derived from the ADEOS-II AMSR. Cooperative plans are being developed by the Aqua and ADEOS-II soil moisture investigstors to jointly utilize the Asian and U.S. SGP sites for validation through shared instrumentation and data exchange.

3.2.4 Quality Control and Diagnostics

Outputs of the retrieval algorithm include two diagnostic parameters: N – the number of iterations required to reach convergence; and χ^2 – the minimum value of chi-squared achieved. Large values of either N or χ^2 are indicators of non-convergence or large errors in the retrievals.

Global fields of the retrieved variables m_e, w_e, and T_e will be created by averaging the output level 2 products onto 10-day and/or monthly grids. The number of samples n, means x_m, and standard deviations s_d, will be computed for each grid point for each variable. The mean fields will be examined for spatial and temporal coherence, the number fields will be examined for missing data, and the standard deviation fields will allow anomalous retrievals to be identified. Tools for routinely scanning and summarizing statistics of these fields will be used.

3.2.5 Exception Handling

The main causes for nonconvergence or errors of the algorithm will be footprints containing residual open water, snow cover, or precipitation. Anomalous inputs due to bad radiometric data (spurious noise, radio-frequency interference, calibration errors, etc.), bad locations, and other lower-level processing errors will be identified. Checks will be made in the processing algorithms to identify remaining anomalies and to assign appropriate flags.

4. CONSTRAINTS, LIMITATIONS, AND ASSUMPTIONS

The retrieval of the specified land products will be limited by the assumptions made in the model, and by the physics of the problem. The following are the major limitations of the output products:

- Footprints may contain mixtures of different surface types, e.g. bare soil, vegetation, rivers. Thus, the retrievals of footprint-averaged soil moisture, temperature, and vegetation, must be interpreted with this in mind. The retrievals nominally represent ~ 70-km area-averages. In cases where there is large contrast (heterogeneity) within a footprint, the retrieved quantities may not accurately represent area-averages due to nonlinearity in the radiative transfer processes. (It is assumed that area-averages are the desired output for large-scale hydrology, climate, and ecological models). This is not expected to be a significant issue based on prior simulations.

- The retrieved variables represent averages over a vertical sampling depth in the medium that is intermediate between the sampling depths at the two frequencies, 6.9 and 10.6 GHz. These depths vary with the amount of moisture in the soil and/or vegetation. The different sampling depths at 6.9 and 10.6 GHz may give rise to some error in the retrievals where the moisture and temperature profiles are highly nonuniform, since each retrieved variable is defined at a single sampling depth.

- As the vegetation cover increases the retrieval errors for m_e and w_e also increase, until at large values of w_e the retrievals become completely unreliable. The vegetation threshholds for reliability of the retrievals are only roughly-defined at this time. Additional simulations prior to launch, and experience with real AMSR data during the post-launch validation phase, will establish these threshholds more precisely.

- Effects of topography, snow cover, clouds, and precipitation, are not explicitly modeled in the retrieval algorithm. Hence, these effects will manifest themselves as errors in the retrievals (if not fully screened out). Topographic effects will not change with time, and may be accounted for in enhanced versions of the baseline algorithm.

5. REFERENCES

Asrar and Greenstone (Eds.) (1995): *1995 MTPE/EOS Reference Handbook*. EOS Project Science Office, NASA Goddard Space Flight Center, Greenbelt, MD.

Beljaars, A. C. M., P. Viterbo, M. J. Miller, and A. J. Betts (1996): The anomalous rainfall over the United States during July 1993: Sensitivity to land surface parameterization and soil moisture anomalies. *Mon. Wea. Rev., 124*, 362-383.

Bengtsson, L., M. Kanamitsu, P. Kallberg, and S. Uppala (1982): FGGE 4-dimensional data assimilation at ECMWF, *Bull. Am. Met. Soc., 63*, 29-43.

Brubaker, K. L. and D. Entekhabi (1996): Analysis of feedback mechanisms in land-atmosphere interaction. *Water Resour. Res., 32*, 1343-1357.

Calvet, J.-C., J.-P. Wigneron, E. Mougin, Y. H. Kerr, and J. S. Brito (1994): Plant water content and temperature of the Amazon forest from satellite microwave radiometry. *IEEE Trans. Geosci. Rem. Sens., 32*, 397-408.

Choudhury, B. J., C. J. Tucker, R. E. Golus, and W. W. Newcomb (1987): Monitoring vegetation using Nimbus-7 scanning multichannel microwave radiometer's data. *Int. J. Rem. Sens., 8*, 533-538.

Choudhury, B. J. and R. E. Golus (1988): Estimating soil wetness using satellite data. *Int. J. Rem. Sens., 9*, 1251-1257.

Choudhury, B. J., E. R. Major, E. A. Smith, and F. Becker (1992): Atmospheric effects on SMMR and SSM/I 37 GHz polarization difference over the Sahel. *Int. J. Rem. Sens., 13*, 3443-3463.

Davis, D. T., Z. Chen, J.-N. Hwang, L. Tsang, and E. G. Njoku (1995): Solving inverse problems by Bayesian iterative inversion of a forward model with applications to parameter mapping using SMMR remote sensing data. *IEEE Trans. Geosci. Rem. Sens., 33*, 1182-1193.

Delworth, T. and S. Manabe (1989): The influence of soil wetness on near-surface atmospheric variability. *J. Clim., 2*, 1447-1462.

Dobson, M. C., F. T. Ulaby, M. T. Hallikainen, and M. A. El-Rayes (1985): Microwave dielectric behaviour of wet soil – Part II: Dielectric mixing models. *IEEE Trans. Geosci. Rem. Sens., GE-23*, 35-46.

Entekhabi, D., H. Nakamura, and E. G. Njoku (1994): Solving the inverse problem for soil moisture and temperature profiles by sequential assimilation of multifrequency remotely sensed observations. *IEEE Trans. Geosci. Rem. Sens., 32*, 438-448.

Ferraro, R. R., N. C. Grody, and J. A. Kogut (1986): Classification of geophysical parameters using passive microwave satellite measurements. *IEEE Trans. Geosci. Rem. Sens., 24,* 1008-1013.

Fung, A. K. and H. J. Eom (1981): Emission from a Rayleigh layer with irregular boundaries. *J. Quant. Spectr. Radiat. Transfer, 26*, 397-409.

Hofer, R. and E. G. Njoku (1981): Regression techniques for oceanographic parameter retrieval using space-borne microwave radiometry. *IEEE Trans. Geosci. Rem. Sens., GE-19*, 178-189.

Jackson, T. J. and T. J. Schmugge (1991): Vegetation effects on the microwave emission from soils. *Rem. Sens. Environ., 36*, 203-212.

Jackson, T. J. (1993): Measuring surface soil moisture using passive microwave remote sensing. *Hydrological Processes, 7*, 139-152.

Jackson, T. J. and D. E. LeVine (1996): Mapping surface soil moisture using an aircraft-based passive microwave instrument: algorithm and example. *J. Hydrology, 184*, 85-99.

Karam, M. A., A. K. Fung, R. H. Lang, and N. S. Chauhan (1992): A microwave scattering model for layered vegetation. *IEEE Trans. Geosci. Rem. Sens., 30*, 767-784.

Kerr, Y. H. and E. G. Njoku (1990): A semiempirical model for interpreting microwave emission from semiarid land surfaces as seen from space. *IEEE Trans. Geosci. Rem. Sens., 28*, 384-393.

Kerr, Y. H. and E. G. Njoku (1993): On the use of passive microwaves at 37 GHz in remote sensing of vegetation. *Int. J. Rem. Sens., 14*, 1931-1943.

Kerr, Y. H. and J. P. Wigneron (1995): Vegetation models and observations - A review. in: *Passive Microwave Remote Sensing of Land-Atmosphere Interactions (B. Choudhury, Y. Kerr, E. Njoku, and P. Pampaloni, Eds.),* VSP, Utrecht, The Netherlands.

LeVine, D. M. and M. A. Karam (1996): Dependence of attenuation in a vegetation canopy on frequency and plant water content. *IEEE Trans. Geosci. Rem. Sens., 34,* 1090-1096.

Lhomme, J. P., A. Chehbouni, and B. Monteny (1994): Effective parameters of surface energy balance in heterogeneous landscapes. *Boundary-Layer Meteorol., 71*, 297-309.

Liou, Y.-A. and A. W. England (1996): Annual temperature and radiobrightness signatures for bare soils. *IEEE Trans. Geosci. Rem. Sens., 34*(4), 981-990.

LoSeen, D., A. Chehbouni, E. Njoku, and S. Saatchi (1995): A modeling study on the use of passive microwave data for the monitoring of sparsely vegetated land surfaces. *Proc. IEEE Geoscience and Remote Sensing Symposium (IGARSS'95),* Florence, Italy.

McFarland, M. J., R. L. Miller, and C. M. U. Neale (1990): Land surface temperature derived from the SSM/I passive microwave brightness temperatures. *IEEE Trans. Geosci. Rem. Sens., 28*(5), 839-845.

Meeson, B. W., F. E. Corprew, J. M. McManus, D. M. Myers, J. W. Closs, K.-J. Sun, D. J. Sunday, and P. J. Sellers (1995): *ISLSCP Initiative I|Global data sets for land-atmosphere models, 1987-1988. Volumes 1-5*. Published on CD by NASA (USA_NASA_GDAAC_ ISLSCP_001 - USA_NASA_GDAACISLSCP_005).

Mo, T., B. J. Choudhury, T. J. Schmugge, J. R. Wang, and T. J. Jackson (1982): A model for microwave emission from vegetation covered fields. *J. Geophys. Res., 87*, 11229-11237.

MTPE (1996): *Mission to Planet Earth Science Strategic Enterprise Plan 1996-2002*, National Aeronautics and Space Administration, Washington, DC.

Neale, C. M. U., M. J. McFarland, and K. Chang (1990): Land-surface-type classification using microwave brightness temperatures from the Special Sensor Microwave/Imager. *IEEE Trans. Geosci. Rem. Sens., 28,* 829-838.

Njoku, E. G. and J. A. Kong (1977): Theory for passive microwave remote sensing of near-surface soil moisture. *J. Geophys. Res., 82*, 3108-3118.

Njoku, E. G. and I. R. Patel (1986): Observations of the seasonal variability of soil moisture and vegetation cover over Africa using satellite microwave radiometry. *Proc. ISLSCP Conference, Rome, Italy, 2-6 December 1985, ESA SP-248*, European Space Agency, Paris, France.

Njoku, E. G., A. Chehbouni, F. Cabot, B. Rague, K. Fleming, and Y. H. Kerr (1994): An approach to estimating surface parameters and fluxes using modeling and multispectral remote sensing. *Proc. IEEE Geoscience and Remote Sensing Symposium (IGARSS'94), Pasadena, California.*

Njoku, E. G. (1995a): Surface temperature estimation over land using satellite microwave radiometry. In: *Passive Microwave Remote Sensing of Land-Atmosphere Interactions (B. J. Choudhury, Y. H. Kerr, E. G. Njoku, and P. Pampaloni, Eds.),* VSP, Utrecht, The Netherlands.

Njoku, E. G., S. J. Hook, and A. Chehbouni (1995b): Effects of surface heterogeneity on thermal remote sensing of land parameters. in: *Scaling Up In Hydrology Using Remote Sensing (J. Stewart, E. Engman, R. Feddes, and Y. Kerr, Eds.),* Wiley, New York.

Norman, J. M. and F. Becker (1995): Terminology in thermal infrared remote sensing of natural surfaces. *Rem. Sens. Rev., 12*, 159-173.

Owe, M., A. Chang, and R. E. Golus (1988): Estimating surface soil moisture from satellite microwave measurements and a satellite-derived vegetation index. *Rem. Sens. Environ., 24*, 131-345.

Owe, M. and A. A. van de Griend (1990): Daily surface moisture model for large area semi-arid land application with limited climate data. *J. Hydrology, 121*, 119-132.

Owe, M., A. A. van de Griend, and A. T. C. Chang (1992): Surface moisture and satellite microwave observations in semiarid southern Africa. *Water Resources Res., 28*, 829-839.

Pitman, A. J. and A. Henderson-Sellers (1996): Simulating the diurnal temperature range: results from Phase 1(a) of the Project for Intercomparison of Landsurface Parameterization Schemes (PILPS), *Atmospheric Research* (in press).

Press, W. H., B. P. Flannery, S. A. Teukolsky, and W. T. Vetterling (1989): *Numerical Recipes* (Ch. 14), Cambridge University Press, New York.

Pulliainen, J. T., J. Grandell, and M. T. Hallikainen (1997): Retrieval of surface temperature in Boreal forest zone from SSM/I data. *IEEE Trans. Geosci. Rem. Sens., 35*, 1188-1200.

Randall, D. A., Harshvardhan, and D. A. Dazlich (1991): Diurnal variability of the hydrologic cycle in a general circulation model. *J. Atmos. Sci., 48*, 40-62.

Raupach, M. R. and J. J. Finnigan (1995): Scale issues in boundary-layer meteorology: surface energy balances in heterogeneous terrain. *Hydrol. Processes, 9*, 589-612.

Shukla, J. and Y. Mintz (1982): Influence of land-surface evapotranspiration on the Earth's climate. *Science, 215*, 1498-1500.

Sippel, S. J., S. K. Hamilton, J. M. Melack, and B. J. Choudhury (1994): Determination of inundation area in the Amazon river floodplain using the SMMR 37 GHz polarization difference. *Rem. Sens. Environ., 48*, 70-76.

Townshend, J. R. G., C. O. Justice, B. J. Choudhury, C. J. Tucker, V. T. Kalb, and T. E. Goff (1989): A comparison of SMMR and AVHRR data for continental land cover characterization. *Int. J. Rem. Sens., 10*, 1633-1642.

Tsang, L. and R. W. Newton (1982): Microwave emission from soils with rough surfaces. *J. Geophys. Res., 87*, 9017-9024.

Tsang, L., J. A. Kong, and R. T. Shin (1985): *Theory of Microwave Remote Sensing*. J. Wiley and Sons, New York.

van de Griend, A. A. and M. Owe (1994): Microwave vegetation optical depth and inverse modelling of soil emissivity using Nimbus/SMMR satellite observations. *Meteorol. Atmos. Phys., 54*, 225-239.

Wang, J. R. and T. J. Schmugge (1980): An empirical model for the complex dielectric permittivity of soil as a function of water content. *IEEE Trans. Geosci. Rem. Sens., GE-18*, 288-295.

Wang, J. R. and B. J. Choudhury (1981): Remote sening of soil moisture content over bare field at 1.4 GHz frequency. *J. Geophys. Res., 86*, 5277-5282.

Wang, J. R. (1985): Effect of vegetation on soil moisture sensing observed from orbiting microwave radiometers. *Rem. Sens. Environ., 17*, 141-151.

Webb, R. S., C. E. Rosenzweig, and E. R. Levine (1992): A global data set of soil particle size properties. Digital raster data on a 1-degree geographic (lat/lon) grid. In: *Global Ecosystems Database Version 1.0: Disc A*, NOAA National Geophysical Data Center, Boulder, CO. 2 independent and one derived spatial layer with 65 attributes, on CD-ROM, 16.5 MB [first published in 1991].

Wegmuller, U., C. Matzler, and E. G. Njoku (1995): Canopy opacity models. *In: Passive Microwave Remote Sensing of Land-Atmosphere Interactions (B. Choudhury, Y. Kerr, E. Njoku, and P. Pampaloni, Eds.),* 375-387, VSP, Utrecht, The Netherlands.

Wei, M.-Y. (1995): *Soil moisture: Report of a workshop held in Tiburon, CA, 25-27 January 1994*. NASA Conference Publication 3319, National Aeronautics and Space Administration, Washington, DC.

Wilheit, T. T. (1978): Radiative transfer in a plane stratified dielectric. *IEEE Trans. Geosci. Rem. Sens., GE-16*, 138-143.

Wilson, M. F. and A. Henderson-Sellers (1985): A global archive of land cover and soil data for use in general circulation climate models, *J. Climatol., 5*, 119-143.

Zurk, L., D. T. Davis, E. G. Njoku, L. Tsang, and J. N. Hwang (1992): Inversion of parameters for semiarid regions by a neural network. *Proc. IEEE Geoscience and Remote Sensing Symposium (IGARSS'92), 1075-1077, Houston, TX, May 1992.*